Cell Reports

Article

Pyruvate metabolism controls chromatin remodeling during CD4+ T cell activation

Graphical abstract

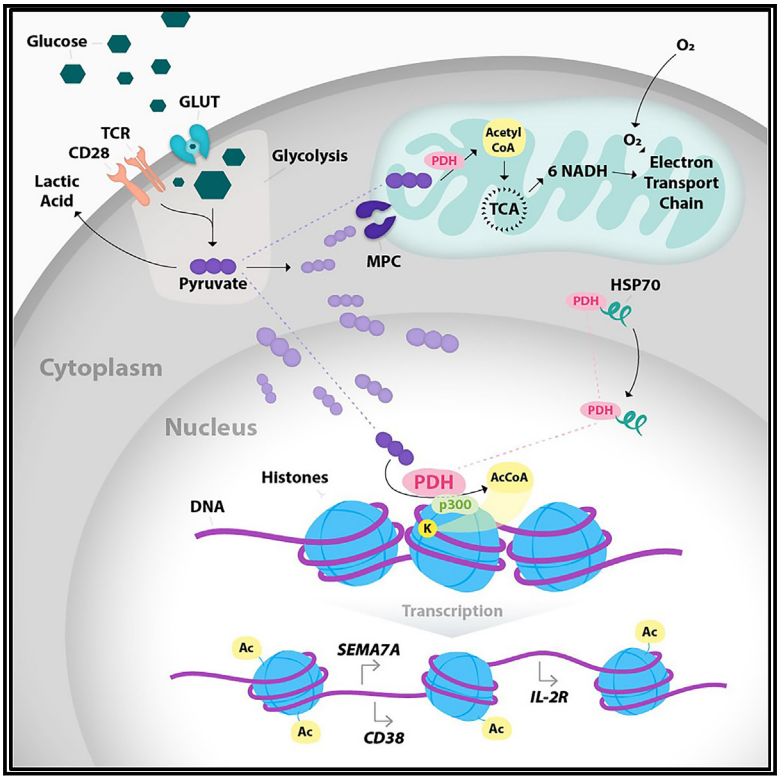

Highlights

- PDH is required for histone acetylation and transcription after T cell activation
- MPC1 and ACLY are not required for T cell activation and transcriptional reprogramming
- T cell activation leads to PDH nuclear translocation close to chromatin-remodeling complexes

Authors

Enric Mocholi, Laura Russo, Keshav Gopal, ..., John Ussher, Boudewijn M.T. Burgering, Paul J. Coffer

Correspondence

e.mocholi-gimeno@umcutrecht.nl (E.M.), p.j.coffer@umcutrecht.nl (P.J.C.)

In brief

After T cell activation, histone acetylation and transcriptional reprogramming require glycolysis and the pyruvate dehydrogenase (PDH)-dependent production of extramitochondrial acetyl-CoA. Mocholi et al. show that PDH translocates to the nucleus close to chromatin-remodeling complexes, highlighting how metabolic and histone-modifying enzymes cooperate in regulating T cell activation.

Mocholi et al., 2023, Cell Reports *42*, 112583
June 27, 2023
https://doi.org/10.1016/j.celrep.2023.112583

CellPress

Cell Reports

CellPress
OPEN ACCESS

Article

Pyruvate metabolism controls chromatin remodeling during CD4$^+$ T cell activation

Enric Mocholi,[1,2,*] Laura Russo,[1,2] Keshav Gopal,[3,14] Andrew G. Ramstead,[4,14] Sophia M. Hochrein,[5,14] Harmjan R. Vos,[1,14] Geert Geeven,[6] Adeolu O. Adegoke,[7] Anna Hoekstra,[8] Robert M. van Es,[1] Jose Ramos Pittol,[1] Sebastian Vastert,[9] Jared Rutter,[4] Timothy Radstake,[9,10] Jorg van Loosdregt,[9] Celia Berkers,[8,11] Michal Mokry,[2,12] Colin C. Anderson,[7] Ryan M. O'Connell,[4,13] Martin Vaeth,[5,13] John Ussher,[3,13] Boudewijn M.T. Burgering,[1,13] and Paul J. Coffer[1,2,15,*]

[1]Center for Molecular Medicine, University Medical Center Utrecht, Utrecht, the Netherlands
[2]Regenerative Medicine Center, University Medical Center Utrecht, Utrecht, the Netherlands
[3]Faculty of Pharmacy and Pharmaceutical Sciences, University of Alberta, Edmonton, AB, Canada
[4]Huntsman Cancer Institute and Division of Microbiology and Immunology, Department of Pathology, University of Utah, 15 N. Medical Drive East, Salt Lake City, UT, USA
[5]Würzburg Institute of Systems Immunology, Max Planck Research Group, Julius-Maximilians University of Würzburg, Würzburg, Germany
[6]Department of Clinical Genetics, Erasmus MC-University Medical Center, Rotterdam, the Netherlands
[7]Department of Surgery, University of Alberta, Edmonton, AB, Canada
[8]Biomolecular Mass Spectrometry and Proteomics, Bijvoet Center for Biomolecular Research, Utrecht University, Utrecht, the Netherlands
[9]Laboratory for Translational Immunology and Department of Pediatric Rheumatology and Immunology, University Medical Center Utrecht, Utrecht, the Netherlands
[10]Department of Rheumatology and Clinical Immunology, University Medical Center Utrecht, Utrecht, the Netherlands
[11]Department of Biochemistry and Cell Biology, Faculty of Veterinary Medicine, Utrecht University, Utrecht, the Netherlands
[12]Cardiovascular Genetics, University Medical Center Utrecht, Utrecht, the Netherlands
[13]These authors contributed equally
[14]These authors contributed equally
[15]Lead contact
*Correspondence: e.mocholi-gimeno@umcutrecht.nl (E.M.), p.j.coffer@umcutrecht.nl (P.J.C.)
https://doi.org/10.1016/j.celrep.2023.112583

SUMMARY

Upon antigen-specific T cell receptor (TCR) engagement, human CD4$^+$ T cells proliferate and differentiate, a process associated with rapid transcriptional changes and metabolic reprogramming. Here, we show that the generation of extramitochondrial pyruvate is an important step for acetyl-CoA production and subsequent H3K27ac-mediated remodeling of histone acetylation. Histone modification, transcriptomic, and carbon tracing analyses of pyruvate dehydrogenase (PDH)-deficient T cells show PDH-dependent acetyl-CoA generation as a rate-limiting step during T activation. Furthermore, T cell activation results in the nuclear translocation of PDH and its association with both the p300 acetyltransferase and histone H3K27ac. These data support the tight integration of metabolic and histone-modifying enzymes, allowing metabolic reprogramming to fuel CD4$^+$ T cell activation. Targeting this pathway may provide a therapeutic approach to specifically regulate antigen-driven T cell activation.

INTRODUCTION

The immune system comprises specialized cell populations that are conditioned to respond rapidly to antigenic and inflammatory signals. While research has focused on these signals in guiding immune responses, emerging data indicate that cellular metabolism is critical in moderating immune cell function and differentiation, consequently influencing the outcome of the adaptive and innate immune response.[1–4] Engagement of the T cell receptor (TCR), concurrent with the recognition of costimulatory molecules by the receptor CD28, triggers T cell activation characterized by transcriptional reprogramming, clonal expansion, and differentiation to effector phenotypes.[5] These changes in the activation status of CD4$^+$ T lymphocytes not only require energy, but also increase demand for metabolic precursors for the biosynthesis of proteins, nucleic acids, and lipids. Therefore, efficient T cell activation requires profound changes in intracellular metabolism.[6,7]

T cell homeostasis is characterized by the metabolism of glucose, fatty acids, and amino acids to generate intermediate metabolites, which can enter the mitochondrial TCA cycle. Upon antigen recognition, T cells rapidly upregulate aerobic glycolysis, but not at the expense of oxidative metabolism, to support bioenergetic demands.[8–10] While the metabolism of proliferating T cells is adapted to facilitate the uptake and incorporation of nutrients into the biomass needed to produce

a daughter cell,[11–13] it has been shown that carbon compound biosynthesis from glucose does not contribute to most of the carbon in proliferating T cells.[14] Hand in hand with activation-induced metabolic changes, epigenome reprogramming (in this paper, the term "epigenome" refers specifically to modifications of histones that can influence gene expression) and regulation of transcriptional output are essential for T cell expansion and differentiation. Underlying this, histone acetylation results in a more accessible chromatin structure permissive to transcriptional machinery. This requires the availability of acetyl-CoA, which is the sole source of acetyl groups in eukaryotic cells.[15] Regulation of the synthesis of acetyl-CoA, which can be produced from acetate, citrate, or pyruvate, serves as a critical rate-limiting step for histone acetyltransferase (HAT) activity within cells.[16–18] Notably, in $CD4^+$ T cells, it has been demonstrated that deletion of lactate dehydrogenase A (LDHA) inhibited glycolytic metabolism, reduced acetyl-CoA levels, and lowered H3K9ac of the *Ifng* enhancer.[19] However, it remains unclear how LDHA deficiency directly modulates acetyl-CoA levels, whether by reducing levels of citrate available for conversion to acetyl-CoA or through inhibition of acetyl-CoA synthetase.[19] Flavell and coworkers have proposed a role for mitochondrial metabolism in regulating H3K9 acetylation in differentiated murine $CD4^+$ Th1 cells.[20] Recently it has also been shown that ATP citrate synthase (ACLY) plays a role in acetyl-CoA generation and epigenome remodeling of T cells during T helper cell (Th) 17 differentiation, specifically through Glut3-mediated uptake of glucose.[21] T cells have also recently been shown to remodel the epigenome by metabolizing acetate in an acetyl-CoA synthetase (ACSS)-dependent manner during conditions of glucose restriction.[22] Furthermore, polyamine metabolism has also been shown to be critical for the ability of $CD4^+$ helper T cells to differentiate, a process that takes several days after initial activation.[23]

$CD4^+$ T cells are metabolically flexible and clearly have multiple mechanisms to ensure acetyl-CoA generation required for epigenome remodeling and transcription. However, it remains unclear whether there is a requirement for specificity in terms of the metabolic pathways that generate (nuclear) acetyl-CoA and whether these pathways play a deterministic role in gene transcription. Here, we have explored the metabolic pathways required for TCR-mediated transcriptional activation during the first 24 h of $CD4^+$ T cell activation. Our results demonstrate that, early after TCR engagement, extramitochondrial pyruvate, as an end-product of glycolysis, but not mitochondrial citrate or exogenous acetate, is driving the remodeling of the $CD4^+$ T cell epigenome. This metabolic-epigenetic crosstalk is critical for the expression of activation-dependent transcription. $CD4^+$ T cell activation also leads to nuclear translocation of pyruvate dehydrogenase and its association with histones and HATs, potentially resulting in localized acetyl-CoA production. Our findings highlight the intimate link between metabolism, transcription, and T cell function. The influence of metabolic alterations in inflammatory environments may allow the design of original interventions to specifically target these pathways, mitigating inflammatory disorders and autoimmunity, in which T cells play a pathophysiological role.

RESULTS

Glucose-derived acetyl-CoA is essential for TCR-induced epigenome remodeling and transcription

T cell activation is known to require a metabolic shift toward glycolysis, triggered by TCR engagement.[6,24] To substantiate the role of glycolysis in transcriptional reprogramming during antigen-driven T cell activation, we utilized a well-established *ex vivo* model to recapitulate the process of antigen stimulation without the requirement for additional antigen-presenting cells.[25,26] We initially explored and validated the conditions for both metabolic and epigenetic reprogramming. Antigen-mediated $CD4^+$ T cell activation initiates context-specific gene-expression programs that drive effector functions and cell fate through changes in the epigenetic landscape.[27] To evaluate global changes in histone modifications, we isolated $CD4^+$ T cells from the peripheral blood (PB) of healthy control (HC) human donors and either maintained them under resting conditions or stimulated with anti-CD3/CD28 for 8, 12, and 24 h. Total levels of H3K27ac, H3K4me1, H3K27me3, and H3K4me3 did not change during the activation (Figures S1A and S1B). However, as expected, rapid changes in the $CD4^+$ epigenome and transcriptome were observed within 24 h as measured by RNA sequencing (RNA-seq) and H3K27ac chromatin immunoprecipitation followed by DNA sequencing (ChIP-seq) (Figures S1C–S1F). Upon T cell activation, increased H3K27ac levels at enhancer-promoters directly correlated with the expression of associated genes (Figures S2A–S2C). Notably, metabolic genes regulating glycolysis also demonstrated both increased activation-induced H3K27ac and increased RNA levels, supporting a positive feedback loop for enforcing and stabilizing metabolic reprogramming (Figures S2D and S2E).

To explore the requirement for metabolic reprogramming in regulating transcriptional responses after initial TCR engagement, $CD4^+$ T cells from PB of healthy donors were isolated and activated either in the presence or absence of oligomycin (inhibitor of ATP synthase blocking the production of ATP by oxidative phosphorylation [OXPHOS]) or 2-deoxyglucose (2DG; competitively inhibiting production of glucose 6-phosphate from glucose) or with replacement of glucose with galactose. Galactose is metabolized through glycolysis, utilizing the Leloir pathway, which is energy neutral, forcing cells to use all the pyruvate production to sustain the TCA cycle for OXPHOS and ATP synthesis at the expense of lactate production.[28–30] We were again unable to detect significant global changes in histone modifications as a consequence of metabolic inhibition (Figures 1A and S3A). According to ChIP-seq and RNA-seq, inhibition of OXPHOS-mediated ATP production by oligomycin had only a limited effect on H3K27 acetylation or activation-induced transcription during the first 24 h of activation (Figures 1B, 1C, and S3B). This is supported by studies that have shown decreased utilization of glucose-derived carbon for mitochondrial metabolism after T cell activation.[8,19] In contrast, inhibition of glycolysis by 2DG treatment compromised both H3K27 acetylation and transcriptional changes (Figures 1B, 1D, and S3C). In the context of murine Th1 cells, the generation of lactate has been found to increase acetyl-CoA levels and H3K9 acetylation at the IFN-γ enhancer.[19] However, under

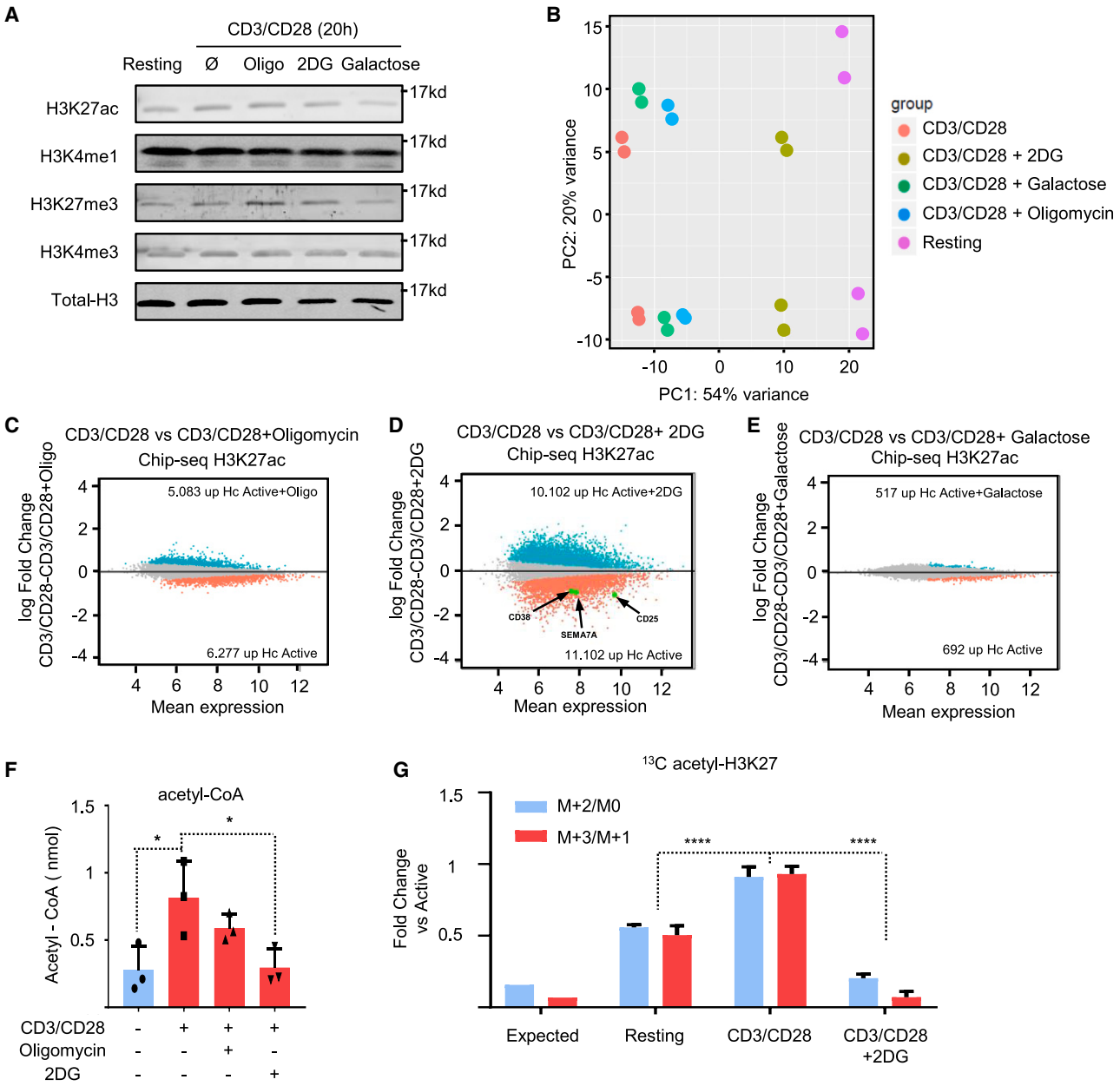

Figure 1. Glycolytic reprogramming is essential for TCR-induced epigenome remodeling and transcription

(A) Immunoblot analysis of acetylated histone H3 (H3K27ac), trimethylated histone H3 at lysine 27 (H3K27me3), trimethylated histone H3 at lysine 4 (H3K4me3), monomethylated histone H3 at lysine 4 (H3K4me1), and global histone H3 levels in human peripheral blood $CD4^+$ T cells after 20-h activation with anti-CD3/CD28 in the presence or absence of oligomycin, 2-deoxyglucose (2DG), or galactose.

(B) Principal components analysis of H3K27ac signal intensity in enhancer regions.

(C–E) MA plots displaying H3K27ac signal intensity at enhancer regions, based on comparisons of replicates within each group. Enhancers with an FDR < 0.05 are marked with red dots.

(F) Acetyl-CoA levels in $CD4^+$ T cells activated for 24 h with anti-CD3/CD28 antibodies, in the absence or presence of oligomycin or 2DG.

(G) LC-MS/MS analysis of the relative levels of acetylated H3K27ac peptide in resting or stimulated T cells, in the absence or presence of 2DG, 24 h after stimulation and resuspension in medium containing 11 mM D-[U-^{13}C]glucose. The M+2/M0 ratio represents the $^{13}C_2$-labeled peptide-to-monoisotopic peptide ratio, while the M+3/M+1 ratio represents the ratio in the case of one additional ^{13}C isotope (serving as a technical replicate). The expected ratio based on the natural abundance of ^{13}C is also indicated.

Data are shown as the mean ± SD of triplicate samples. *p < 0.05, ****p < 0.0001 (ANOVA). Each dot on the graphs represents an independent experiment.

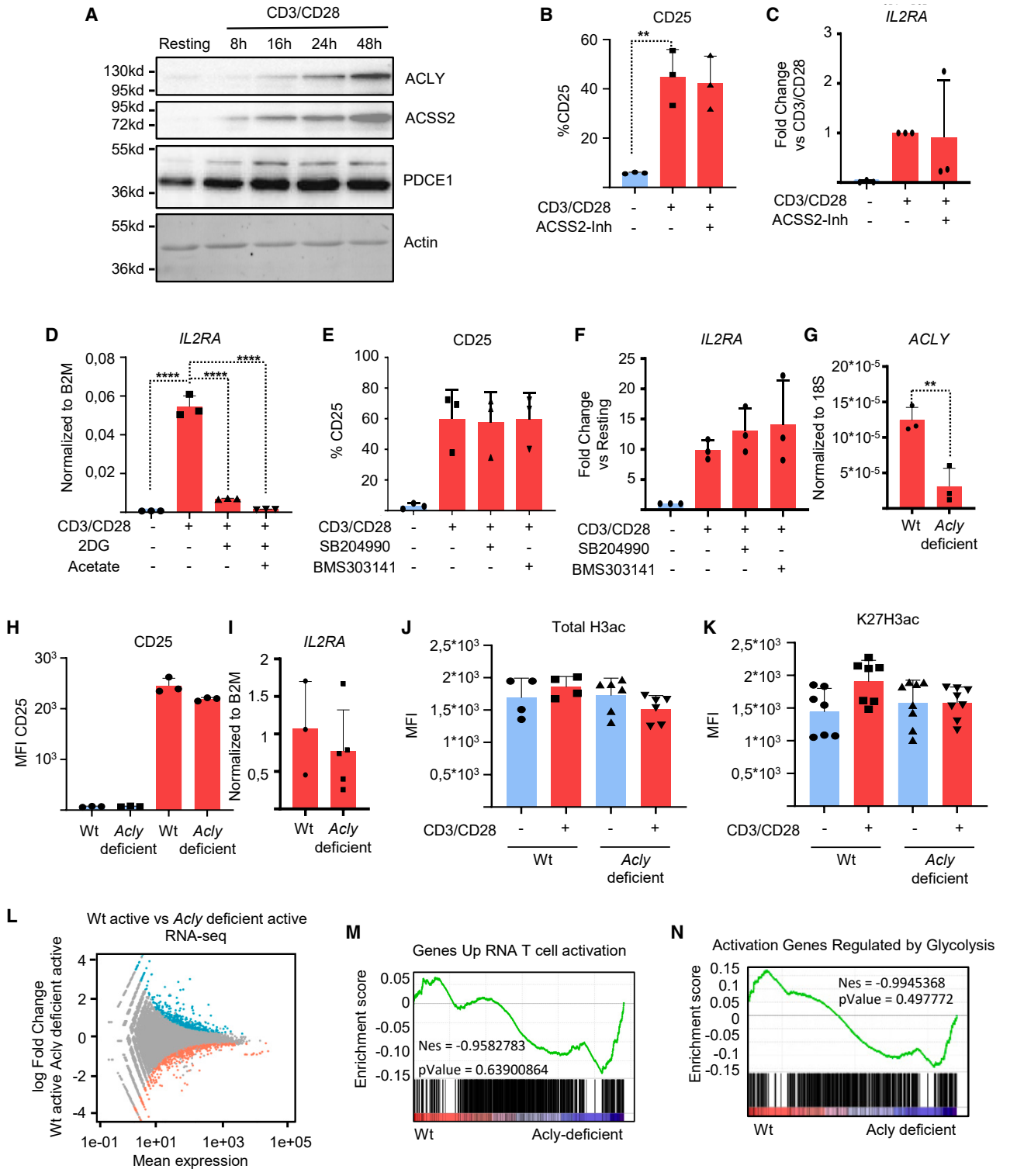

Figure 2. ACSS2 inhibition or ACLY deficiency does not affect epigenome remodeling during T cell activation

(A) Immunoblots of ACLY, ACSS2, PDCE1, and actin from human T cells activated for 8, 16, 24, or 48 h with anti-CD3/CD28 stimulation.

(B and C) CD25 protein expression was measured by flow cytometry (FACS) and *IL2ra* gene expression was determined by quantitative reverse transcription-polymerase chain reaction (qRT-PCR) in human $CD4^+$ T cells activated with anti-CD3/CD28 in the presence and absence of ACSS2 inhibitor (15.6 μM).

(legend continued on next page)

conditions of galactose metabolism, where lactate production is abrogated, activated CD4$^+$ T cells were still able to globally remodel H3K27 acetylation and reprogram the transcriptome (Figures 1B, 1E, S3D, and S10B). Principal components analysis (PCA) of H3K27ac ChIP-seq and RNA-seq analyses suggests that activation-induced H3K27ac changes and transcription are dependent on glycolysis but not the production of lactate (Figures 1B and S3E).

Identification of activation-induced genes, as defined by increased H3K27 acetylation ($\leq$5 kb away from their transcription start site [TSS]), in the absence or presence of 2DG, identified a subset that depends on increased glycolysis (Figure S3F). Gene ontology (GO)-term analysis reveals that these are critical players in T cell activation and include interleukin receptors, CD markers, and other genes associated with T cell activation (Figures S4A and S4B). *IL2RA*, *SEMA7A*, and *CD38* are examples of this group of genes and were used as surrogate activation markers for further analysis (Figure S4C). To validate that these genes are dependent on glycolysis during T cell activation, we activated human CD4$^+$ T cells in the presence of 2DG or the absence of glucose and measured cell-surface and RNA expression of CD25, CD38, or SEMA7A (Figure S4D). Access to glucose and initiation of glycolysis are clear requirements for the expression of these genes.

To evaluate the role of glucose-derived acetyl-CoA in changes in H3K27ac we first measured acetyl-CoA levels in CD4$^+$ T cells under resting or activated conditions in the presence or absence of oligomycin or 2DG. Increased acetyl-CoA levels were observed after activation and were primarily dependent on glycolytic metabolism (Figure 1F). In addition, human T cells were stimulated with anti-CD3/CD28 in the presence of heavy glucose (D-[$^{13}C_6$]glucose), and the levels of isotopically coded acetyl groups on H3K27 were measured by liquid chromatography-mass spectrometry (LC-MS). CD4$^+$ T cell activation resulted in an increase in $^{13}C_2$ incorporation in acetylated H3K27 histones that was abrogated by the addition of 2DG (Figures 1G and S4E). Taken together, these data demonstrate that during the early phase of antigen-driven T cell activation, glycolysis is essential for acetyl-CoA production, H3K27ac-mediated chromatin remodeling, and transcriptional reprogramming, independent of lactate production.

Acetate and citrate metabolism is not required for TCR-induced epigenome remodeling

To evaluate the potential role of intermediate glycolytic metabolites in the generation of acetyl-CoA and histone remodeling, we first evaluated the expression levels of enzymes generating acetyl-CoA. Human CD4$^+$ T cells were stimulated with anti-CD3/CD28, and the levels of ACLY, acyl-coenzyme A synthetase short-chain family member 2 (ACSS2), and pyruvate dehydrogenase alpha 1 (PDCE1) were measured (Figures 2A and S5A). Expression of ACLY and ACSS2 was low in resting cells and during the first 16 h of activation, but increased after 24 h of stimulation. In contrast, PDCE1 expression was already present in resting cells and was subsequently upregulated. A recent study provided evidence that T cells activated for 5 or 9 days are also able to remodel the epigenome in an ACSS-dependent manner during glucose restriction.[22] To evaluate this in the first 24 h of activation, T cells were activated in the presence or absence of an inhibitor of ACSS2. Inhibition of ACSS2 did not prevent TCR-mediated increases in CD25, protein, or mRNA expression during this first 24 h of activation (Figures 2B and 2C). To further validate that ACSS2 is not essential during the first 24 h of activation to remodel the epigenome, we analyzed H3K27 acetylation. Pharmacological inhibition of ACSS2 did not affect H3K27ac levels (Figure S5B). Furthermore, the provision of exogenous acetate during 24 h of T cell activation was insufficient to rescue *IL2RA* expression under conditions where glycolysis was inhibited (Figure 2D). To evaluate the effects of the inhibition of ACCS2 on T cell function, T cells were activated for 5 days in the presence or absence of an ACCS2 inhibitor. Cytokine production (IL-2 and IFN-γ) and proliferation were evaluated by ELISA or fluorescence-activated cell sorting (FACS), respectively. ACCS2 inhibition did not affect either proliferation or cytokine production (Figures S5C, S5D, and S6A).

To evaluate the role of ACLY in transcriptional reprogramming, human CD4$^+$ T cells were activated for 24 h in the presence or absence of an ACLY inhibitor (SB204990 or BMS303141). Cell-surface protein and mRNA expression of CD25, CD38, or SEMA7A were again evaluated. ACLY inhibition did not prevent TCR-mediated expression, supporting the notion that citrate-derived acetyl-CoA is not required for the transcriptional regulation of T cells during the first 24 h of activation (Figures 2E, 2F, S6B, and S6C). To further validate that ACLY is not essential during the first 24 h of activation to remodel the epigenome, we again analyzed H3K27ac. Inhibition of ACLY did not affect H3K27ac (Figure S5B). We also evaluated the effects of ACLY inhibition on cytokine production (IL-2 and IFN-γ) and proliferation. Human T cells were activated for 5 days in the presence or absence of an ACLY inhibitor (SB204990). ACLY inhibition did not have any effect on

(D) *Il2ra* gene expression was determined by qRT-PCR in human CD4$^+$ T cells activated with anti-CD3/CD28 in the presence and absence of 2DG or 2DG with acetate (20 mM).

(E and F) CD25 protein expression was measured by FACS and *Il2ra* gene expression was determined by qPCR in human CD4$^+$ T cells activated with anti-CD3/CD28 in the presence and absence of ACLY inhibitors (SB204990 [5 μM] and BMS303141 [30 μM]).

(G) *Acly* gene expression by naive murine CD4$^+$ T cells 24 h after *in vitro* activation with anti-CD3/CD28 was measured by qRT-PCR.

(H) CD25 expression was measured as a percentage on naive murine CD4$^+$ T cells 24 h after *in vitro* activation with anti-CD3 and anti-CD28.

(I) *Il2ra* gene expression was determined by qRT-PCR in naive murine CD4$^+$ T cells 24 h after *in vitro* activation with anti-CD3/CD28.

(J and K) Mean fluorescence intensity of total acetylation histone 3 and acetylation histone 3 K27 was measured in naive murine CD4$^+$ T cells 24 h after *in vitro* activation with anti-CD3 and anti-CD28.

(L) Differentially expressed genes were analyzed by means of MA plots, with red dots indicating enhancers with a false discovery rate (FDR) < 0.1.

(M and N) Gene set enrichment analysis was performed to compare upregulated T cell activation gene sets and T cell activation regulated by glycolysis gene sets between wild-type and ACLY-deficient activated T cells. Data are shown as the mean ± SD of triplicate samples. $^{**}p < 0.01$, $^{****}p < 0.0001$ (ANOVA or t test). Each dot on the graphs represents an independent experiment.

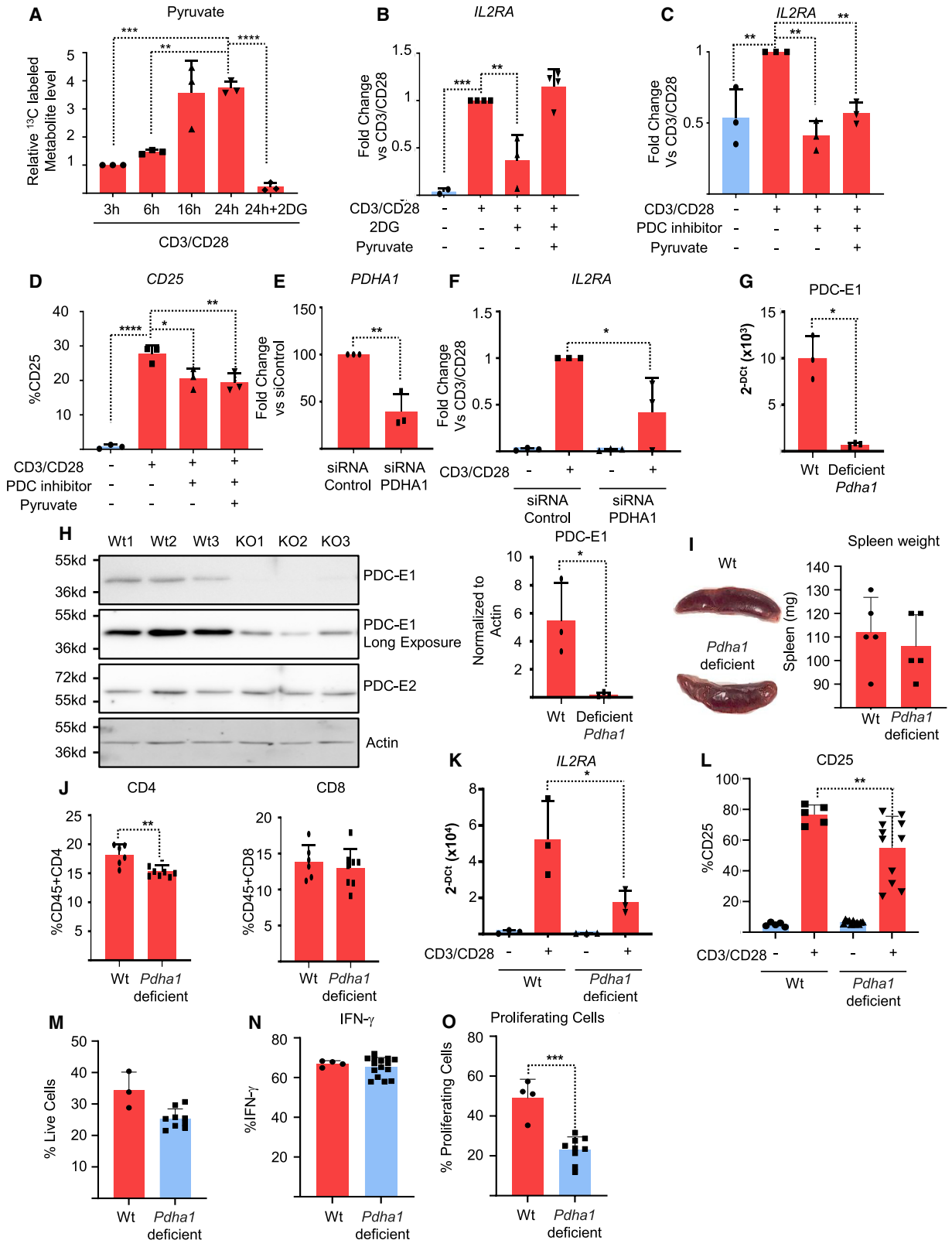

(legend on next page)

proliferation or cytokine production (Figures S5C, S5D, and S6A).

As previously mentioned, a role for glucose-derived citrate in Th17 epigenetic reprogramming has recently been described.[21] To genetically confirm that ACLY is not required for activation-induced epigenome remodeling within the first 24 h, we utilized $CD4^+$ T cells from conditional knockout mice with T cell-specific ablation of ACLY (CD4-Cre $ACLY^{fl/fl}$) (Figure 2G). To evaluate the impact of the loss of ACLY in regulating transcriptional responses after TCR engagement, *Acly*-deficient or wild-type (WT) $CD4^+$ T cells were stimulated with anti-CD3/CD28, and expression of CD25 was evaluated (Figures 2H and 2I). *ACLY* deletion did not affect TCR-mediated upregulation of CD25 expression. To substantiate the notion that ACLY activity is also not essential to remodel the epigenome during the first 24 h of activation, we analyzed global histone 3 (H3) acetylation and acetylation at H3K27 by flow cytometry and observed that the absence of ACLY does not affect the levels of total H3 or H3K27ac (Figures 2J, 2K, S7A, and S7B). We subsequently performed global transcriptomics using RNA-seq. The absence of ACLY had a limited effect on activation-induced transcription during the first 24 h of activation (Figures 2L and S7C). In addition, gene set enrichment analysis (GSEA) demonstrated that the transcriptional changes observed after *ACLY* deletion do not correlate with genes upregulated during the first 24 h of T cell activation or with genes downregulated upon inhibition of glycolysis (Figures 2M and 2N). These data confirm that ACLY is not required for transcriptional regulation during the initial phase of human and mouse $CD4^+$ T cell activation. Taken together these data show that histone acetylation and gene expression in the initial phase of T cell activation depend neither on acetate nor on citrate metabolism.

Pyruvate dehydrogenase is required for activation-induced transcriptional reprogramming and T cell function

Although glycolysis is central in driving chromatin remodeling and transcriptional reprogramming during the first 24 h of T cell activation, our data suggest that neither ACSS2 nor ACLY plays a critical role. To evaluate the role of pyruvate metabolism, we first evaluated intracellular pyruvate levels during T cell activation. $CD4^+$ T cells were stimulated with anti-CD3/CD28 in the presence of D-[$^{13}C_6$]glucose, and intracellular [^{13}C]pyruvate levels were measured by LC-MS (Figure 3A). Maximal pyruvate levels were observed 16 h after activation. To evaluate whether pyruvate is a critical glycolytic intermediate regulating the expression of activation-induced genes, we performed a rescue experiment by activating $CD4^+$ T cells in the presence or absence of 2DG or 2DG together with pyruvate. The addition of pyruvate was sufficient to rescue *IL2RA*-, *CD38*-, and *SEMA7A*-associated H3K27 acetylation under conditions where glycolysis was inhibited (Figures 3B and S7D).

To evaluate whether pyruvate dehydrogenase (PDH) is critical for activation-induced histone acetylation, we utilized 6,8-bis(benzylthio)octanoic acid, an inhibitor of PDH activity.[31] $CD4^+$ T cells activated in presence of 6,8-bis(benzylthio)octanoic acid showed no increase in *CD25*-, *SEMA7A*-, and *CD38*-associated H3K27 promoter acetylation (Figures 3C and S7E) and reduced cell-surface expression of these markers (Figures 3D and S7F). Furthermore, the addition of pyruvate was no longer sufficient to rescue *CD25*-, *CD38*-, and *SEMA7A*-associated H3K27 promotor acetylation or cell-surface expression (Figures 3C, 3D, and S7E). To confirm that inhibition of PDH affects epigenome remodeling, we evaluated H3K27ac. Pharmacological inhibition of PDH has a clear effect on the levels of H3K27ac (Figure S5B). To further evaluate the

Figure 3. Absence of PDH activity affects T cell function

(A) Analysis of intracellular ^{13}C-labeled pyruvate in T cells using LC-MS after stimulation with or without 2-deoxyglucose (2DG). Samples were collected at 3, 6, 16, and 24 h after stimulation, and cells were incubated in medium containing 11 mM D-[U-^{13}C]glucose.

(B) H3K27ac ChIP-qPCR of *Il2ra* enhancer regions in human $CD4^+$ T cells. Cells were activated with anti-CD3/CD28 antibodies and treated with 2DG alone or 2DG with pyruvate (2 mM) or were untreated as a control. The results show the effect of these treatments on the levels of H3K27ac modification in the *Il2ra* enhancer regions.

(C) ChIP-qPCR of the *Il2ra* enhancer region in human $CD4^+$ T cells. Cells were activated with anti-CD3/CD28 antibodies and treated with 6,8-bis(benzylthio) octanoic acid (PDC inhibitor) alone or PDC inhibitor with pyruvate (2 mM) or were untreated as a control.

(D) Flow cytometry analysis of CD25 expression in human $CD4^+$ T cells activated with anti-CD3/CD28 antibodies. Cells were treated with 6,8-bis(benzylthio) octanoic acid (PDC inhibitor) alone or PDC inhibitor with pyruvate or were untreated as a control.

(E and F) qRT-PCR analysis of mRNA expression of *Pdha1* and *Il2ra* in human $CD4^+$ T cells. Cells were transfected with siRNA targeting *Pdha1* or a control siRNA and activated 24 h later.

(G) Expression levels of *Pdha1* in $CD4^+$ T cells isolated from wild-type (WT) and *Pdha1*-deficient mice.

(H) Immunoblots and quantification of PDCE1, PDCE2, and actin in murine $CD4^+$ T cells from WT or *Pdha1*-deficient mice.

(I) Representative images of spleens from WT and *Pdha1*-deficient mice. Comparison of the weight of spleens in WT and *Pdha1*-deficient mice. The results show any morphological differences between the spleens of the two genotypes and the effect of *Pdha1* deficiency on spleen weight.

(J) Flow cytometry analysis of $CD4^+$ and $CD8^+$ T cell subpopulations in the spleens of *Pdha1*-deficient mice and their $CD4^{CreERT2}$ littermate controls at 6 weeks of age.

(K) qRT-PCR analysis of *Il2ra* gene expression in naive murine $CD4^+$ T cells 24 h after activation with anti-CD3/CD28 antibodies. The results show the impact of *Pdha1* deficiency on the T cell subpopulations in the spleen and the effect of *in vitro* activation on *Il2ra* gene expression in $CD4^+$ T cells.

(L) Percentage of positive CD25 on naive murine $CD4^+$ T cells 24 h after *in vitro* activation with anti-CD3 and αCD28. Data are representative of multiple experiments.

(M) Flow cytometry analysis of cell viability of $CD4^+$ T cells activated with anti-CD3/CD28 antibodies for 5 days using Zombie Green.

(N) Flow cytometry analysis of IFN-γ production by $CD4^+$ T cells activated with anti-CD3/CD28 antibodies for 5 days.

(O) Flow cytometry analysis of $CD4^+$ T cell proliferation after 5 days of activation with anti-CD3/CD28 antibodies, measured using CellTrace violet. All graphs represent the mean ± SD. Statistical significance was measured by one-way ANOVA, Student's t test, or Mann-Whitney test of the area under the curve for EAE clinical score. *$p < 0.05$, **$p < 0.01$, ***$p < 0.001$, ****$p < 0.0001$. Each dot on the graphs represents an independent experiment.

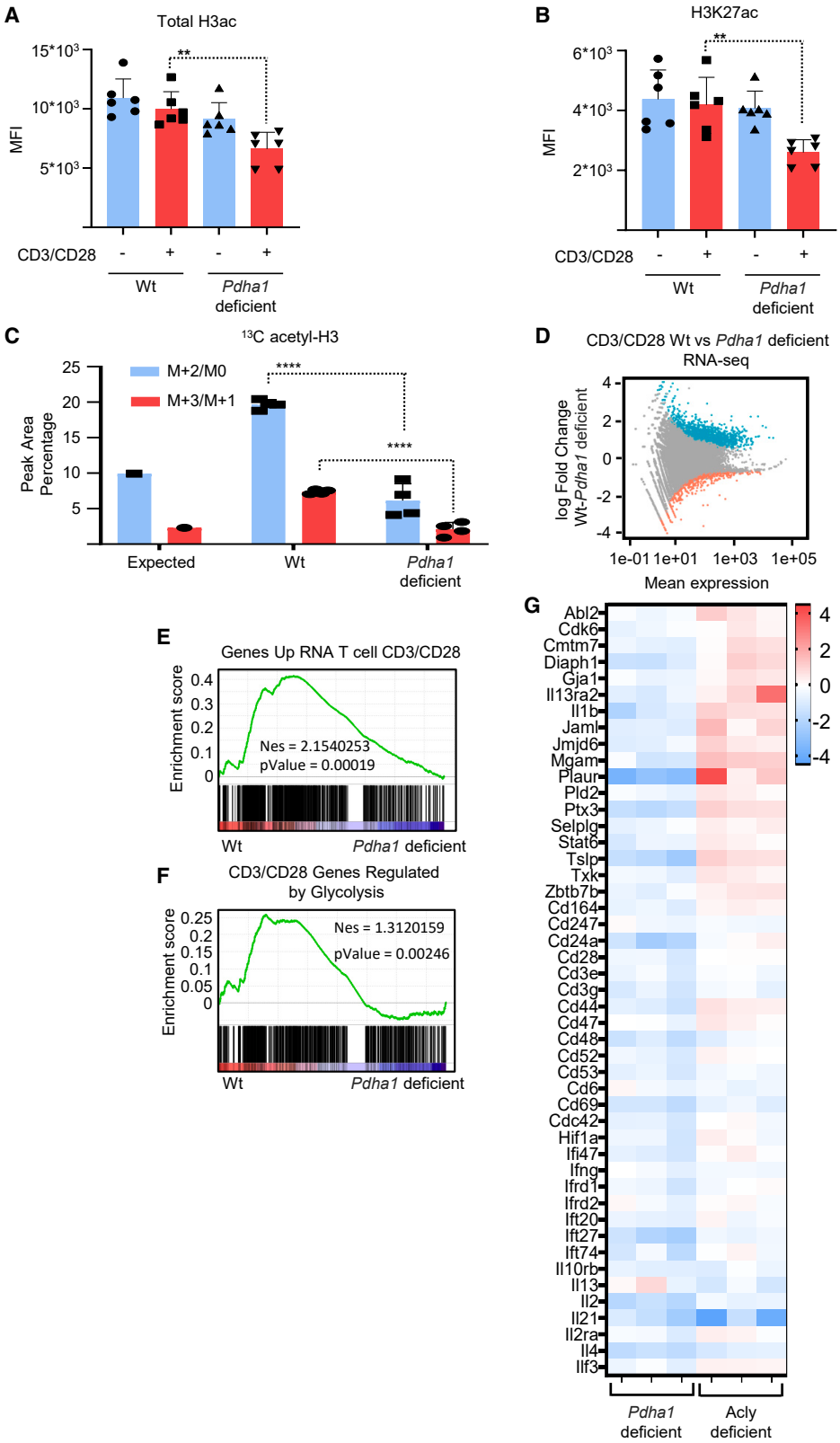

(legend on next page)

effect of PDH inhibition on T cell function, T cells were activated for 5 days in the presence or absence of 6,8-bis(benzylthio)octanoic acid. While we observed that PDH inhibition did not reduce IL-2 or IFN-γ production (Figures S6B and S6C), proliferation was significantly inhibited (Figures S6A). To further validate our inhibitor data, we performed small interfering RNA (siRNA)-mediated knockdown of *Pdha1*, an essential subunit of the PDH complex, in human CD4$^+$ T cells. With an efficiency of around 50% (Figure 3E), *Pdha1* knockdown in CD4$^+$ T cells showed a clear decrease in the expression of *IL2RA*, *SEMA7A*, and *CD38* (Figures 3F and S7G).

To confirm that PDH plays a fundamental role in activation-induced transcriptional reprogramming of CD4$^+$ T cells, we generated an inducible T cell-specific *Pdha1*-knockout mouse by crossing *Pdha1*$^{fl/fl}$ mice with CD4^{CreERT2}. To induce *Pdha1* deletion, animals were treated with tamoxifen for 5 days, and after 3 weeks, a reduction in *Pdha1* mRNA and PDCE1 protein was observed (Figures 3G and 3H). The expression of PDCE1 was greatly reduced, although not eliminated, while the expression of PDCE2 was unaffected (Figure 3H). *Pdha1*$^{fl/fl}$CD4^{CreERT2} mice had a normal spleen size and weight (Figure 3I), and there were no significant differences in splenic populations of CD45, CD8, or myeloid-lineage cells or neutrophils compared with WT mice (Figures 3J and S8A). A small but significant reduction in the total number of CD4$^+$ T cells and a moderate increase in naive CD4$^+$ T cells were observed (Figures 3J and S8A). In addition, *Pdha1* deletion resulted in a clear reduction in T-regulatory (Treg) cells (FoxP3$^+$) compared with the WT animals (Figure S8A). The effect of *Pdha1* deletion on T cell metabolism was evaluated by Seahorse extracellular flux analyses. Activated T cells showed a moderate but significant reduction in mitochondrial respiration and maximal respiration (Figures S8B–S8D). This demonstrates that under these conditions, the TCA cycle can be supported independently of pyruvate metabolism. In addition, disruption of the PDH does not have a significant effect on glycolytic lactate production (Figure S8E).[32] To investigate the effect of T cell-specific PDH disruption on T cell function, *Pdha1*-deficient or WT CD4$^+$ T cells were stimulated with anti-CD3/CD28 for 24 h, and mRNA expression and CD25 cell-surface protein were evaluated (Figures 3K and 3L). *Pdha1* deletion resulted in a decrease in both *IL2RA* and CD25 expression compared with CD4^{ERT2} controls. This decrease in CD25 expression could not be rescued by the addition of extra pyruvate (Figure S8F). In addition, *Pdha1*-deficient or WT CD4$^+$ T cells were stimulated with anti-CD3/CD28 for 5 days, and the viability, proliferation, and IFN-γ production were measured by FACS. Similar to our observations with human CD4$^+$ T cells, *Pdha1* deficiency did not have an impact on viability or IFN-γ production (Figures 3M, 3N, and S9A); however, T cell proliferation was significantly reduced (Figures 3O and S9B).

We wanted to explore the impact of T cell-specific PDC disruption on the regulation of epigenome remodeling and transcriptional responses after TCR engagement. First, we analyzed global H3 acetylation and H3K27 acetylation by FACS. We observed that the absence of *Pdha1* decreased the levels of total H3 and H3K27ac (Figures 4A, 4B, S9C, and S9D). To substantiate the notion that PDH-derived acetyl-CoA is utilized for epigenetic remodeling, we measured the incorporation of glucose-derived ^{13}C carbons into histones as described above. In *Pdha1*-deficient T cells, we detected significantly less incorporation of ^{13}C in the histone fraction, demonstrating the requirement for PDH activity in glucose-dependent histone modification (Figures 4C and S9E). We subsequently performed global transcriptomics using RNA-seq. *Pdha1* deficiency compromised transcriptome reprogramming during T cell activation (Figure 4D). There was a clear correlation between the expression of genes affected by the loss of *Pdha1* and genes that are upregulated during T cell activation and downregulated in the presence of 2DG (Figures 4E and 4F). Importantly, in the evaluation of the expression of a subset of T cell activation marker genes, loss of *Pdha1*, but not *Acly*, was detrimental (Figure 4G). Taken together, these data support an essential role for PDH activity in driving CD4$^+$ T cell activation and transcriptional reprogramming.

Mitochondrial pyruvate transport is not required for activation-induced epigenome remodeling and CD4$^+$ T cell function

In eukaryotes, the biosynthesis of acetyl-CoA is thought to occur in the subcellular compartment where it is required, since it is both membrane-impermeable and unstable, due to the high-energy thioester bond that joins the acetyl and CoA groups.[28,33–35] The major role of PDH is to metabolize pyruvate to acetyl-CoA in the mitochondria, driving the TCA cycle. To explore this, we activated human CD4$^+$ T cells in the presence or absence of 2DG, (2E)-3-(3-pyridinyl)-1-(4-pyridinyl)-2-propen-1-one (3PO; PFKFB3 inhibitor), UK5099 (mitochondrial pyruvate carrier inhibitor), or dichloroacetate (DCA; PDH kinase [PDK] inhibitor) (Figures S10A–S10C). No drug-induced differences in CD4$^+$ T cell viability were observed (Figures S11A–S11C). ChIP-qPCR analysis revealed that activation of CD4$^+$ T cells in the presence of 2DG or 3PO (inhibitors of glycolysis) prevented *CD25*-, *CD38*-, or *SEMA7A*-associated

Figure 4. PDH is required for epigenome remodeling after T cell activation

(A) Mean fluorescence intensity of total histone 3 acetylation in naive murine CD4$^+$ T cells 24 h after *in vitro* activation with anti-CD3/CD28.

(B) Mean fluorescence intensity of H3K27ac in naive murine CD4$^+$ T cells 24 h after *in vitro* activation with anti-CD3/CD28.

(C) Analysis of the incorporation of ^{13}C carbons derived from glucose into histones of activated WT and *Pdha1*-deficient T cells, with means ± SEM calculated from four mice.

(D) MA plot of differentially expressed genes, based on comparisons of all replicates between activated WT T cells and activated *Pdha1*-deficient T cells. Red dots indicate enhancers with an FDR < 0.1.

(E) Gene set enrichment analysis between upregulated T cell activation gene set and WT versus *Pdha1*-deficient RNA-seq.

(F) Gene set enrichment analysis between T cell activation regulated by glycolysis gene set and WT versus *Pdha1*-deficient RNA-seq.

(G) Heatmap of T cell activation genes with significant differential expression between *Pdha1*-deficient or *Acly*-deficient CD4$^+$ T cells and activated WT CD4$^+$ T cells. All graphs represent the mean ± SD. Statistical significance was measured by one-way ANOVA. **p < 0.01, ****p < 0.0001. Each dot on the graphs represents an independent experiment.

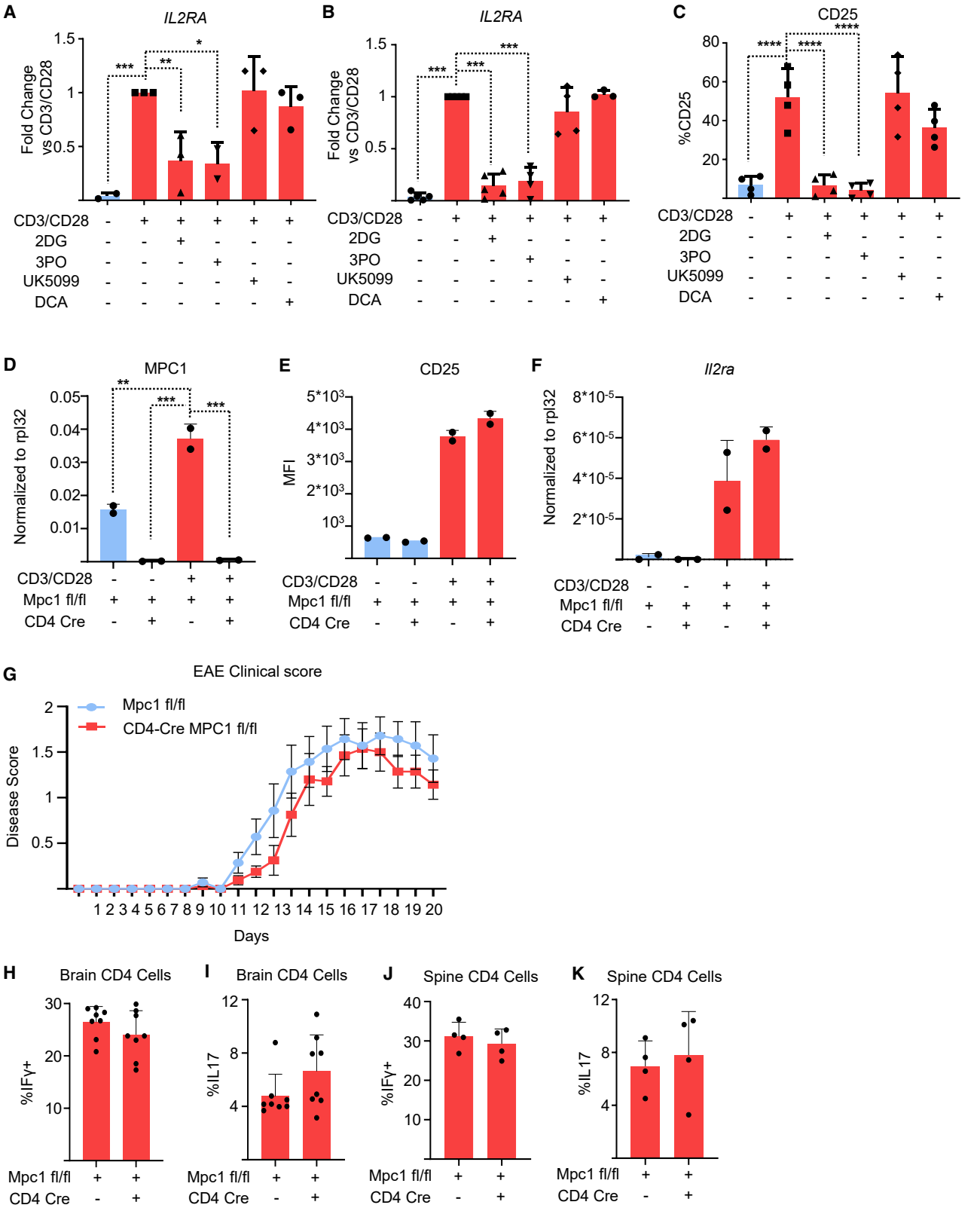

(legend on next page)

H3K27 acetylation and transcription (Figures 5A, 5B, S12A, and S12B) and inhibited cell-surface protein expression (Figures 5C and S12C). $CD4^+$ T cells activated in the presence of DCA (which promotes TCA cycle metabolism, thereby reducing lactate production) or in the presence of UK5099 (inhibitor of mitochondrial pyruvate import and promotor of lactate production) showed no effect (Figures 5A–5C and S12A–S12C). To additionally validate that transport of pyruvate to mitochondria is not essential during the first 24 h of activation to remodel the epigenome, we analyzed H3K27ac in the presence of UK5099. Pharmacological inhibition of MPC1 did not affect H3K27ac (Figure S5B). To eliminate the possibility that MPC2 was working as an autonomous membrane carrier,[36] T cells were activated in the presence of the thiazolidinedione derivative rosiglitazone, which can inhibit MPC2 activity.[37,38] Rosiglitazone treatment also did not affect TCR-mediated increases in CD25, CD38, or SEMA7A protein or mRNA expression (Figure S13A).

These data support a mechanism whereby the generation of pyruvate, but not mitochondrial transport and subsequent metabolism, is critical for T cell-mediated activation. To further confirm this, we utilized $CD4^+$ T cells from a conditional Mpc1-deficient mouse model (CD4-Cre $Mpc1^{fl/fl}$).[39] $CD4^+$ T cells from Mpc1-knockout (KO) or WT mice were stimulated with anti-CD3/CD28 for 24 h. The levels of *Mpc1* expression were analyzed by qRT-PCR, confirming Mpc1 deletion in $CD4^+$ T cells from CD4-Cre $Mpc1^{fl/fl}$ animals (Figure 5D). Under the same conditions the surface expression of CD25 and CD69, another early activation marker, was evaluated (Figures 5E and S13B). Transcription of *Il2ra* and *Sema7a* was also evaluated by qRT-PCR (Figures 5F and S13C). Mpc1 deletion did not affect TCR-mediated increases in either transcription or protein expression, demonstrating that mitochondrial pyruvate transport is not required for transcriptional regulation of these genes in *in vitro*-activated $CD4^+$ T cells.

We subsequently evaluated the requirement for mitochondrial pyruvate transport on $CD4^+$ T cell function and the impact of the loss of Mpc1 on peripheral T cell responses. To this end, we utilized the experimental autoimmune encephalomyelitis (EAE) model. Mice lacking Mpc1 in T cells have normal evolution of disease compared with WT (Figure 5G). At the endpoint of the experiment, leukocytes were isolated from the brain and spine, and IFN-γ and IL-17A production by $CD4^+$ T cells was analyzed by flow cytometry (Figures 5H–5K). Consistent with disease scores, our results show that the same percentages of IFN-γ- and IL-17-producing $CD4^+$ T cells infiltrated brains and spines of WT and CD4-Cre $Mpc1^{fl/fl}$ animals. These data further confirm that Mpc1-deficient $CD4^+$ T cells are functional and able to migrate to the inflammatory locus and amplify the immune reaction.

Collectively, these data validate that, during T cell activation, glycolytic pyruvate production, but not its subsequent transport into mitochondrial, is essential for the epigenomic remodeling and effector function of $CD4^+$ T cells.

TCR engagement induces PDC nuclear translocation and histone association required for epigenome remodeling and transcription

The PDC has been reported to translocate to the nucleus in a heat shock protein (Hsp70)-dependent manner.[34] To evaluate the relevance of PDH translocation during T cell activation, nuclei were isolated from human $CD4^+$ T cells stimulated with anti-CD3/CD28 for 24 h in the presence or absence of 2DG. PDCE1, encoded by *PDHA1*, was detected by immunoblotting, and levels in the nucleus were found to increase during activation in a glycolysis-independent manner (Figures S13D and S13E). To determine whether nuclear transport of PDCE1 was indeed Hsp70 dependent, human $CD4^+$ T cells were stimulated with anti-CD3/CD28 for 24 h in the presence or absence of KNK437, which results in decreased expression of inducible Hsp70.[40] KNK437 decreased nuclear levels of PDCE1 (Figure 6A), without affecting $CD4^+$ T cell viability (Figures S11A–S11C). To evaluate whether Hsp70 plays a role in TCR-induced transcription, we activated human $CD4^+$ T cells in the presence or absence of KNK437 and measured the cell-surface expression of CD25, CD38, or SEMA7A. Hsp70 inhibition prevented TCR-mediated increases in CD25, CD38, and SEMA7A expression, correlating with reduced nuclear PDCE1 expression (Figures 6B and 6C).

The molecular mechanism by which acetyl-CoA is made available for histone acetylation at the level of chromatin is still not well defined. Based on our observations, a potential mechanism could involve direct interaction between PDH subunits and histones or HATs such as p300. To determine whether the PDC complex may interact with histones or p300, we performed a

Figure 5. Mitochondrial pyruvate metabolism is not required for epigenome remodeling after T cell activation

(A) The *Il2ra* enhancer region of human $CD4^+$ T cells activated with anti-CD3/CD28 was analyzed by ChIP-qPCR in the absence or presence of 2DG, 3PO, UK5099, or DCA.

(B) The mRNA expression of *Il2ra* was measured by qRT-PCR in human $CD4^+$ T cells activated with anti-CD3/CD28 in the absence or presence of 2DG, 3PO, UK5099, or DCA.

(C) The expression of CD25 protein was analyzed by flow cytometry in human $CD4^+$ T cells activated with anti-CD3/CD28 in the absence or presence of 2DG, 3PO, UK5099, or DCA.

(D) The gene expression of *Mpc1* in naive murine $CD4^+$ T cells 24 h after *in vitro* activation with anti-CD3/CD28 was measured by qRT-PCR.

(E) The mean fluorescence intensities of CD25 on naive murine $CD4^+$ T cells 24 h after *in vitro* activation with anti-CD3 and anti-CD28 were analyzed by flow cytometry. These results are representative of multiple experiments.

(F) The gene expression of *Il2ra* by naive murine $CD4^+$ T cells 24 h after *in vitro* activation with anti-CD3/CD28 was measured by qRT-PCR.

(G) The clinical scores during EAE were measured and are presented as mean values from two separate experiments, each with n = 14 mice per group.

(H and I) The percentage of $CD4^+$ T cells in the brains of EAE mice expressing IL-17A and IFN-γ was analyzed by flow cytometry at day 20.

(J and K) The percentage of $CD4^+$ T cells in the spines of EAE mice expressing IL-17A and IFN-γ was analyzed by flow cytometry at day 20. All graphs represent the mean ± SD. Statistical significance was measured by one-way ANOVA or Student's t test. *$p < 0.05$, **$p < 0.01$, ***$p < 0.001$, ****$p < 0.0001$. Each dot on the graphs represents an independent experiment.

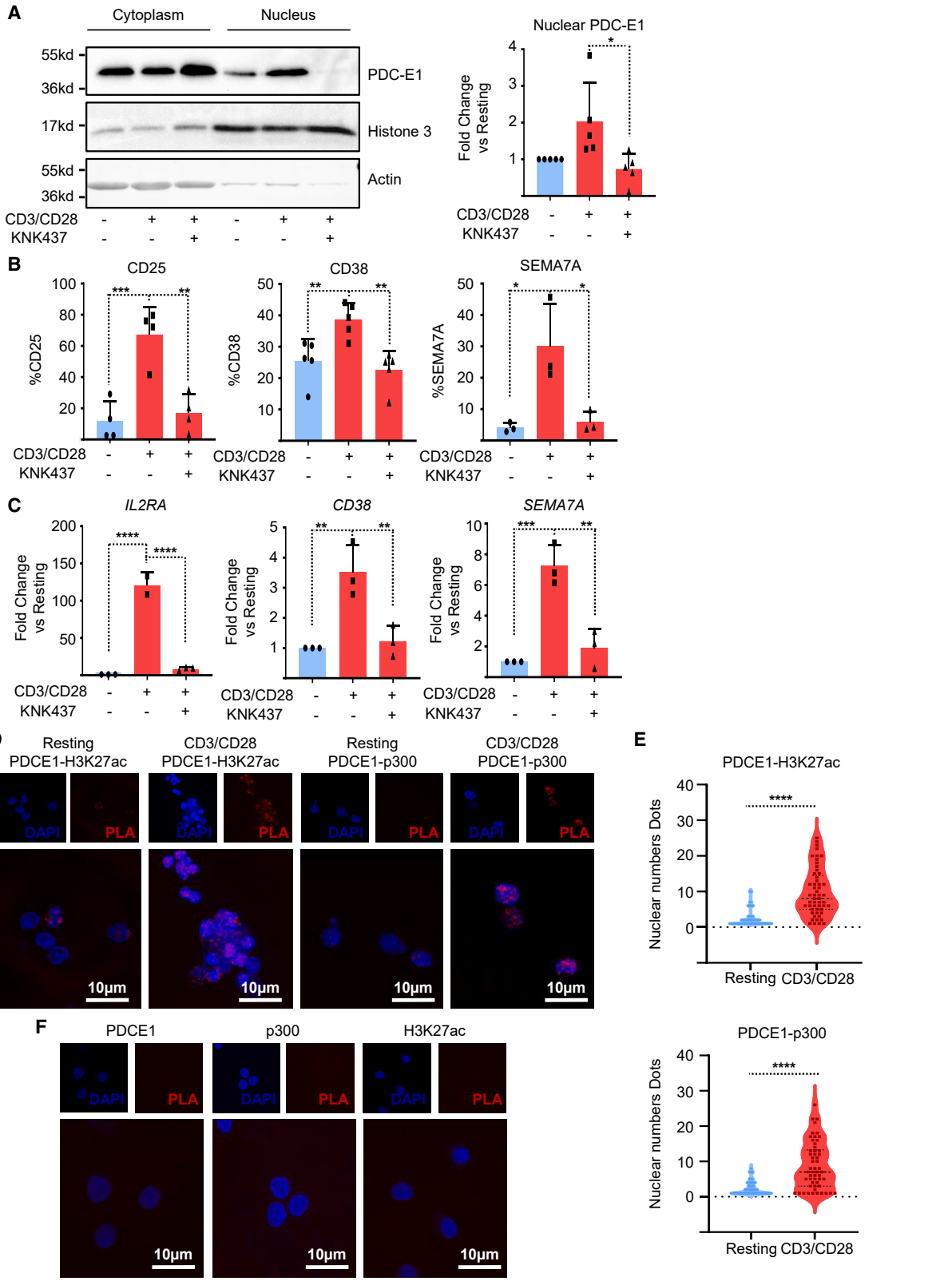

(legend on next page)

proximity ligation assay (PLA) enabling the detection of protein-protein interactions in T cells, as we have previously described.[41,42] The colocalization of PDCE1 and p300, or PDCE1 and H3K27ac, was observed in the nucleus, further supporting our western blot localization data (Figures 6D–6F). Notably, the association of PDCE1 with p300 and PDCE1 with H3K27ac was dependent on T cell activation, suggesting that PDC shuttles into the nucleus upon antigenic stimulation.

Taken together, these data support a model where T cell activation results in Hsp70-mediated nuclear translocation of PDC and association with chromatin.

DISCUSSION

Despite sufficient oxygen being present for the generation of ATP by mitochondrial respiration, when T lymphocytes encounter antigen, they undergo metabolic reprogramming to exploit aerobic glycolysis.[6,43–45] What remains unclear is how glycolytic intermediates are specifically utilized during these early stages of T cell activation. Clearly, activation-induced glucose uptake plays important roles in T cell development, proliferation, and function.[8,28,33,46–49] The switch to glycolysis is considered necessary to facilitate carbon incorporation into the biomass that is required during the acute and rapid expansion of T cells upon activation.[11,12] However, recent data have challenged this concept, showing that carbon biosynthesis from glucose does not contribute to most of the carbon in proliferating murine T lymphocytes.[14] Furthermore, while $CD4^+$ T cells can use either OXPHOS or glycolysis to fuel proliferation, this can also proceed in the absence of aerobic glycolysis.[28] These and other observations suggest that glycolysis is essential for intracellular processes in addition to generating intracellular building blocks and energy production. Here, we show that activation of $CD4^+$ T cells results in epigenetic and transcriptional reprogramming that is dependent on glycolysis to generate extramitochondrial pyruvate, with its subsequent metabolism to acetyl-CoA by PDH. This occurs in parallel with the nuclear translocation of PDH and its subsequent association with histones and HAT. These observations provide novel insights into the early stages of $CD4^+$ T cell activation, helping to explain why increased glucose uptake is required for T cell proliferation and development and demonstrating specificity in terms of the metabolic pathways required for these events.

In eukaryotes, acetyl-CoA is produced in the subcellular compartment where it is required.[34] Thus, regulation of nuclear acetyl-CoA production likely serves as a critical step in the regulation of epigenome remodeling.[17] This is supported in studies of *Saccharomyces cerevisiae* where nuclear acetyl-CoA synthesis is rate limiting for histone acetylation.[50] Our data show that, during T cell activation, carbons derived from glucose are incorporated into acetylated histones (Figure 1G), providing a direct link between glycolysis and *de novo* histone acetylation required to remodel the epigenome. Deletion of the glycolytic enzyme LDHA in $CD4^+$ T cells has been shown to inhibit glycolysis, reduce acetyl-CoA levels, and lower H3K9ac levels at the IFN-γ enhancer.[19] However, this study focused on H3K9ac and did not explore global transcriptional reprogramming. It also remains unclear how LDHA deficiency directly modulates acetyl-CoA levels. A 30% reduction in glucose uptake was observed in LDHA-KO animals, which could in itself affect H3K9ac through mechanisms we have described here. In contrast, our data demonstrate that activation of T cells in the presence of galactose or DCA,[28] inhibiting the conversion of pyruvate to lactate, does not affect H3K27ac levels or transcription during T cell activation (Figures 1E, 5A–5C, and S12A–S12C). This suggests that inhibition of lactate production does not have an impact on H3K27ac enhancer remodeling after TCR engagement.

While acetyl-CoA can be produced from acetate, citrate, or pyruvate, how this is regulated and whether specificity is important during the early phase of T cell activation remain important and currently unanswered questions. Here, we show that blocking mitochondrial pyruvate transport, or inhibiting ACLY and ACSS2 during the first 24 h of activation, did not affect activation-induced H3K27ac or transcription (Figures 2B–2N and 5A–5F). We have also shown that inhibition of mitochondrial pyruvate transport abrogates T cell activation-induced OXPHOS and reduces citrate levels (Figure S10C and Ramstead et al.[39]). This supports the concept that neither citrate, acetate, nor mitochondrial intermediate metabolites are required for epigenetic remodeling. Instead, our data support a model whereby extramitochondrial pyruvate synthesis is crucial for epigenome remodeling, rather than TCA cycle intermediary products. This is supported by a recent study by Menk et al. in which it was shown that upregulation of PDH kinase 1 (PDHK1) activity, preventing mitochondrial import of pyruvate, is acutely required for T cell activation-induced cytokine synthesis.[51] T cells have been recently reported to utilize acetate to remodel the epigenome in an ACSS-dependent manner, but this was specifically under conditions of glucose restriction and activating the T cells for 5 or 9 days.[22] Our data also show that, in the presence of glucose, ACSS2 inhibition does not affect transcriptome remodeling during T cell activation (Figures 2B and 2C). In addition, the provision of exogenous acetate during T cell activation was not sufficient to rescue epigenome remodeling when glycolysis

Figure 6. TCR engagement regulates PDH nuclear translocation and chromatin association

(A) Representative immunoblots and quantification of PDCE1 localization in the nucleus of human $CD4^+$ T cells activated with anti-CD3/CD28 antibodies, with and without the Hsp70 inhibitor KNK437 (100 μM).

(B and C) Measurement of CD25, CD38, and SEMA7A expression by flow cytometry (FACS) and qRT-PCR in human $CD4^+$ T cells activated with anti-CD3/CD28, with and without the Hsp70 inhibitor KNK437 (100 μM).

(D and E) Proximity ligation assay (PLA) analysis of PDCE1's association with H3K27ac and p300 in resting human $CD4^+$ T cells and in cells activated with anti-CD3/CD28 antibodies for 24 h.

(F) PLA negative control for PDCE1, H3K27ac, and p300 in human $CD4^+$ T cells activated with anti-CD3/CD28 antibodies for 24 h. All graphs represent the mean ± SD. Statistical significance was measured by one-way ANOVA or Student's t test. *$p < 0.05$, **$p < 0.01$, ***$p < 0.001$, ****$p < 0.0001$. Each dot on the graphs represents an independent experiment.

was inhibited (Figure 2D). A role for mitochondrial metabolism and polyamine metabolism has also been described to regulate epigenetic changes during the differentiation of $CD4^+$ T cells into Th cell subsets.[20,21,23] However, these studies examined murine lymphocytes several days after activation-induced differentiation. Taking our data into account further highlights the large degree of flexibility exhibited by $CD4^+$ T cells in exploiting metabolic changes to drive chromatin remodeling.

PDH has been shown to play a role in the thymic maturation of T cells, and it was proposed that it does not have a role in T cell numbers downstream of the double-positive stage of differentiation.[32] However, during the submission of this article, a study provided *in vivo* data demonstrating a role for PDH in the proliferation, survival, and function of Th17 cells.[52] Mice with a T cell-specific deletion of PDH were less susceptible to developing EAE and clearly showed a functional role for PDH in regulating T cell homeostasis. The absence of PDH affected citrate levels, interfering with OXPHOS, lipid synthesis, and histone acetylation, all of which are crucial for the transcription of Th17 signature genes.[52] Our inducible KO model showed a small but significant change in the number of $CD4^+$ T cells in the spleen and a reduced number of Treg cells (Figures 3J and S8A). Soriano-Baguet et al. also reported a decrease in the number of Treg cells in the brains of PDH-deficient animals in the EAE model; these observations provide evidence for a wider involvement of PDH in $CD4^+$ Th-subset differentiation.[52] However, we have demonstrated that, within the first 24 h of TCR engagement, PDH is necessary for transcriptional reprogramming, independent of pyruvate translocation to the mitochondria or citrate levels (Figure 4). This was also essential for T cell activation (Figures 3I and 3J), and these results further highlight the metabolic flexibility of T cells. Mitochondrial PDC has previously been reported to be present and functional in the nucleus of fibroblasts. Knockdown of nuclear PDH components in isolated functional nuclei decreased the *de novo* synthesis of acetyl-CoA and acetylation of core histones.[34] Our data demonstrate that in T cells, PDCE1, a subunit of the PDH complex, is translocated to the nucleus in an Hsp70-dependent manner during $CD4^+$ T cell activation (Figure 6A). Inhibition of nuclear translocation or depletion of PDCE1 prevented activation-induced changes in $CD4^+$ T cell transcription (Figures 4A–4G, 6B, and 6C). Furthermore, we demonstrated that PDH can be in close proximity to both H3K27ac and the p300 acetyltransferase upon T cell activation, and by this mechanism could maintain higher local acetyl-CoA concentrations at specific enhancers and promotors. This association between PDH, histones, and p300 is also regulated in a TCR-activation-dependent manner and may be critical in directing the rapid changes in enhancer activation and transcription observed in $CD4^+$ T cells after initial TCR engagement (Figures 6D–6F).

Our data demonstrate a clear specificity in the use of intermediate metabolites in the generation of acetyl-CoA, chromatin remodeling, and transcriptional reprogramming after $CD4^+$ T cell activation. Furthermore, the association of PDH subunits with histones and HATs suggests a potentially deterministic role in driving the specificity of enhancer activation. The tight integration of metabolic enzymes with histones and chromatin-modifying enzymes allows metabolic reprogramming to fuel acute and rapid changes in transcriptional output. While our data have focused on the early stages of $CD4^+$ T cell activation, these findings could be applicable to a variety of systems where metabolism drives changes in cell fate.

Limitations of the study

(1) Our study evaluates the role of the catalytic subunit of PDH in the essential histone modifications required for transcriptome changes during T cell activation. However, this focuses primarily on the initial 24-h period of T cell activation. We did not investigate the consequences of PDH absence on the differentiation of different T cell subsets or on prolonged T cell activation in this particular study. Furthermore, as our study specifically focuses on short-term T cell activation, we did not evaluate the impact of PDH absence on autoimmune disease models *in vivo*. (2) We have focused exclusively on the histone modification H3K27ac, which is a marker of open enhancers. While we demonstrate that glycolysis and PDH are essential for this histone modification during T cell activation, there are multiple histone modifications that contribute to the epigenome. We have not assessed the impact that inhibiting glycolysis or the absence of PDH might have on other histone modifications. Further research is needed to explore the effects of these interventions on other histone modifications and their potential contributions to T cell activation. (3) Our study revealed that, during T cell activation, PDH is translocated to the nucleus in an HSP70-dependent manner, and this translocation is crucial for the production of acetyl-CoA. While we also observed that inhibiting HSP70 has a potent effect on the histone modifications induced during this process, we recognize that HSP70 has other functions than translocating PDH to the nucleus. Thus, it will be necessary to investigate further the details of PDH translocation to the nucleus or explore alternative ways to specifically inhibit PDH in the nucleus without affecting its function in the cytoplasm.

STAR★METHODS

Detailed methods are provided in the online version of this paper and include the following:

- KEY RESOURCES TABLE
- RESOURCE AVAILABILITY
  - Lead contact
  - Materials availability
  - Data and code availability
- EXPERIMENTAL MODEL AND STUDY PARTICIPANT DETAILS
  - Pdha1 T cell-specific KO mice
  - MPC1 T cell-specific KO mice
  - ACLY T cell-specific KO mice
  - Collection of PB samples
- METHOD DETAILS
  - Human T cell isolation and culture
  - Chromatin-immunoprecipitation
  - DNA/RNA-sequencing
  - ChIP-qPCR
  - Detection of apoptosis
  - Immunoblotting

- Real-time PCR
- Seahorse assay
- Measurements of acetyl-coA levels
- Measurement of pyruvate levels using liquid chromatography-mass spectrometry (LC-MS) based metabolomics
- Incorporation of glucose-derived carbons in histones measured by liquid chromatography-mass spectrometry (LC-MS) based proteomics
- Proximity ligation assay (PLA)
- Isolation and culture of mouse naïve CD4$^+$ T cells
- ChIP-seq analysis

● QUANTIFICATION AND STATISTICAL ANALYSIS

SUPPLEMENTAL INFORMATION

Supplemental information can be found online at https://doi.org/10.1016/j.celrep.2023.112583.

ACKNOWLEDGMENTS

We are grateful to all the authors of this paper for their contributions and significant effort in completing and publishing this research. We would like to extend a special thank you to J.U. and K.G. (Alberta University) for their assistance in generating the Pdca1-KO mice, which were essential to the study's success. We would like to express our gratitude to M.V. at the Würzburg Institute for generously providing us with the ACLY KO needed to validate our hypothesis. We would also like to thank H.R.V. and R.M.v.E. from the proteomic facility of the UMC for their scientific discussions and for their assistance with the challenging experiments involving carbon tracing of heavy carbons from glucose that are incorporated into histone modifications. Their expertise and exceptional problem-solving skills were instrumental in the success of this study. We would also like to express our gratitude to R.M.O. from Utah University for providing us with valuable data from the MPC1-KO mice. In conclusion, we would also like to extend our gratitude to G.G. and M.M. for their invaluable assistance with the RNA-seq and ChIP-seq analyses performed in this study. Finally, we would like to thank all members of the Coffer Lab for their valuable discussions concerning this work. This work is supported by the Stichting WKZ Foundation (2016) and ReumaNetherlands (NR 18- 01-401).

AUTHOR CONTRIBUTIONS

The experiments were mainly performed by E.M. with the assistance of L.R. J.U. and K.G. contributed by generating the Pdha1-KO mice and were involved in some experiments using this mouse model. A.G.R., J.R., and R.M.O. conducted all the experiments with the MPC1 KO mice. The metabolomics studies were conducted by S.M.H. and C.B., while H.R.V. and R.M.v.E. performed carbon tracing of heavy carbons from glucose incorporated into histone modifications. G.G. and M.M. analyzed the RNA-seq and ChIP-seq data. A.O.A. and C.C.A. conducted the EAE model with the Pdha1 mouse model, which was not included in the final version of the paper. During the study, S.M.H. and M.V. played a crucial role by providing us with the ACLY KO and conducting some of the experiments with this mouse model. The scientific discussions led by J.R., S.V., T.R., J.v.L., and B.M.T.B. were highly valuable in generating hypotheses and improving the overall experimental design. The study was designed and written by E.M. and P.J.C.

DECLARATION OF INTERESTS

The authors declare no competing interests.

INCLUSION AND DIVERSITY

We support inclusive, diverse, and equitable conduct of research.

Received: January 12, 2023
Revised: February 17, 2023
Accepted: May 15, 2023
Published: June 1, 2023

REFERENCES

1. Jacobs, S.R., Herman, C.E., Maciver, N.J., Wofford, J.A., Wieman, H.L., Hammen, J.J., and Rathmell, J.C. (2008). Glucose uptake is limiting in T cell activation and requires CD28-mediated Akt-dependent and independent pathways. J. Immunol. *180*, 4476–4486.
2. Araki, K., Turner, A.P., Shaffer, V.O., Gangappa, S., Keller, S.A., Bachmann, M.F., Larsen, C.P., and Ahmed, R. (2009). mTOR regulates memory CD8 T-cell differentiation. Nature *460*, 108–112.
3. Man, K., Miasari, M., Shi, W., Xin, A., Henstridge, D.C., Preston, S., Pellegrini, M., Belz, G.T., Smyth, G.K., Febbraio, M.A., et al. (2013). The transcription factor IRF4 is essential for TCR affinity-mediated metabolic programming and clonal expansion of T cells. Nat. Immunol. *14*, 1155–1165.
4. Freemerman, A.J., Johnson, A.R., Sacks, G.N., Milner, J.J., Kirk, E.L., Troester, M.A., Macintyre, A.N., Goraksha-Hicks, P., Rathmell, J.C., and Makowski, L. (2014). Metabolic reprogramming of macrophages: glucose transporter 1 (GLUT1)-mediated glucose metabolism drives a proinflammatory phenotype. J. Biol. Chem. *289*, 7884–7896.
5. Vaeth, M., Maus, M., Klein-Hessling, S., Freinkman, E., Yang, J., Eckstein, M., Cameron, S., Turvey, S.E., Serfling, E., Berberich-Siebelt, F., et al. (2017). Store-operated Ca(2+) entry controls clonal expansion of T cells through metabolic reprogramming. Immunity *47*, 664–679.e6.
6. Frauwirth, K.A., Riley, J.L., Harris, M.H., Parry, R.V., Rathmell, J.C., Plas, D.R., Elstrom, R.L., June, C.H., and Thompson, C.B. (2002). The CD28 signaling pathway regulates glucose metabolism. Immunity *16*, 769–777.
7. Bauer, D.E., Harris, M.H., Plas, D.R., Lum, J.J., Hammerman, P.S., Rathmell, J.C., Riley, J.L., and Thompson, C.B. (2004). Cytokine stimulation of aerobic glycolysis in hematopoietic cells exceeds proliferative demand. Faseb. J. *18*, 1303–1305.
8. Wang, R., Dillon, C.P., Shi, L.Z., Milasta, S., Carter, R., Finkelstein, D., McCormick, L.L., Fitzgerald, P., Chi, H., Munger, J., and Green, D.R. (2011). The transcription factor Myc controls metabolic reprogramming upon T lymphocyte activation. Immunity *35*, 871–882.
9. O'Neill, L.A.J., Kishton, R.J., and Rathmell, J. (2016). A guide to immunometabolism for immunologists. Nat. Rev. Immunol. *16*, 553–565.
10. Wang, Y., Tao, A., Vaeth, M., and Feske, S. (2020). Calcium regulation of T cell metabolism. Curr. Opin. Physiol. *17*, 207–223.
11. Vander Heiden, M.G., Cantley, L.C., and Thompson, C.B. (2009). Understanding the Warburg effect: the metabolic requirements of cell proliferation. Science *324*, 1029–1033.
12. Vander Heiden, M.G., Lunt, S.Y., Dayton, T.L., Fiske, B.P., Israelsen, W.J., Mattaini, K.R., Vokes, N.I., Stephanopoulos, G., Cantley, L.C., Metallo, C.M., and Locasale, J.W. (2011). Metabolic pathway alterations that support cell proliferation. Cold Spring Harbor Symp. Quant. Biol. *76*, 325–334.
13. Lunt, S.Y., and Vander Heiden, M.G. (2011). Aerobic glycolysis: meeting the metabolic requirements of cell proliferation. Annu. Rev. Cell Dev. Biol. *27*, 441–464.
14. Hosios, A.M., Hecht, V.C., Danai, L.V., Johnson, M.O., Rathmell, J.C., Steinhauser, M.L., Manalis, S.R., and Vander Heiden, M.G. (2016). Amino acids rather than glucose account for the majority of cell mass in proliferating mammalian cells. Dev. Cell *36*, 540–549.
15. Choudhary, C., Weinert, B.T., Nishida, Y., Verdin, E., and Mann, M. (2014). The growing landscape of lysine acetylation links metabolism and cell signalling. Nat. Rev. Mol. Cell Biol. *15*, 536–550.
16. Su, X., Wellen, K.E., and Rabinowitz, J.D. (2016). Metabolic control of methylation and acetylation. Curr. Opin. Chem. Biol. *30*, 52–60.
17. Kinnaird, A., Zhao, S., Wellen, K.E., and Michelakis, E.D. (2016). Metabolic control of epigenetics in cancer. Nat. Rev. Cancer *16*, 694–707.

18. Campbell, S.L., and Wellen, K.E. (2018). Metabolic signaling to the nucleus in cancer. Mol. Cell *71*, 398–408.

19. Peng, M., Yin, N., Chhangawala, S., Xu, K., Leslie, C.S., and Li, M.O. (2016). Aerobic glycolysis promotes T helper 1 cell differentiation through an epigenetic mechanism. Science *354*, 481–484.

20. Bailis, W., Shyer, J.A., Zhao, J., Canaveras, J.C.G., Al Khazal, F.J., Qu, R., Steach, H.R., Bielecki, P., Khan, O., Jackson, R., et al. (2019). Distinct modes of mitochondrial metabolism uncouple T cell differentiation and function. Nature *571*, 403–407.

21. Hochrein, S.M., Wu, H., Eckstein, M., Arrigoni, L., Herman, J.S., Schumacher, F., Gerecke, C., Rosenfeldt, M., Grün, D., Kleuser, B., et al. (2022). The glucose transporter GLUT3 controls T helper 17 cell responses through glycolytic-epigenetic reprogramming. Cell Metabol. *34*, 516–532.e11.

22. Qiu, J., Villa, M., Sanin, D.E., Buck, M.D., O'Sullivan, D., Ching, R., Matsushita, M., Grzes, K.M., Winkler, F., Chang, C.H., et al. (2019). Acetate promotes T cell effector function during glucose restriction. Cell Rep. *27*, 2063–2074.e5.

23. Puleston, D.J., Baixauli, F., Sanin, D.E., Edwards-Hicks, J., Villa, M., Kabat, A.M., Kamiński, M.M., Stanckzak, M., Weiss, H.J., Grzes, K.M., et al. (2021). Polyamine metabolism is a central determinant of helper T cell lineage fidelity. Cell *184*, 4186–4202.e20.

24. Frauwirth, K.A., and Thompson, C.B. (2004). Regulation of T lymphocyte metabolism. J. Immunol. *172*, 4661–4665.

25. Trickett, A., and Kwan, Y.L. (2003). T cell stimulation and expansion using anti-CD3/CD28 beads. J. Immunol. Methods *275*, 251–255.

26. Sagerström, C.G., Kerr, E.M., Allison, J.P., and Davis, M.M. (1993). Activation and differentiation requirements of primary T cells in vitro. Proc. Natl. Acad. Sci. USA. *90*, 8987–8991.

27. Roh, T.Y., Cuddapah, S., Cui, K., and Zhao, K. (2006). The genomic landscape of histone modifications in human T cells. Proc. Natl. Acad. Sci. USA. *103*, 15782–15787.

28. Chang, C.H., Curtis, J.D., Maggi, L.B., Jr., Faubert, B., Villarino, A.V., O'Sullivan, D., Huang, S.C.C., van der Windt, G.J.W., Blagih, J., Qiu, J., et al. (2013). Posttranscriptional control of T cell effector function by aerobic glycolysis. Cell *153*, 1239–1251.

29. Holden, H.M., Rayment, I., and Thoden, J.B. (2003). Structure and function of enzymes of the Leloir pathway for galactose metabolism. J. Biol. Chem. *278*, 43885–43888.

30. Aguer, C., Gambarotta, D., Mailloux, R.J., Moffat, C., Dent, R., McPherson, R., and Harper, M.E. (2011). Galactose enhances oxidative metabolism and reveals mitochondrial dysfunction in human primary muscle cells. PLoS One *6*, e28536.

31. Zachar, Z., Marecek, J., Maturo, C., Gupta, S., Stuart, S.D., Howell, K., Schauble, A., Lem, J., Piramzadian, A., Karnik, S., et al. (2011). Non-redox-active lipoate derivates disrupt cancer cell mitochondrial metabolism and are potent anticancer agents in vivo. J. Mol. Med. *89*, 1137–1148.

32. Jun, S., Mahesula, S., Mathews, T.P., Martin-Sandoval, M.S., Zhao, Z., Piskounova, E., and Agathocleous, M. (2021). The requirement for pyruvate dehydrogenase in leukemogenesis depends on cell lineage. Cell Metabol. *33*, 1777–1792.e8.

33. Shi, L.Z., Wang, R., Huang, G., Vogel, P., Neale, G., Green, D.R., and Chi, H. (2011). HIF1alpha-dependent glycolytic pathway orchestrates a metabolic checkpoint for the differentiation of TH17 and Treg cells. J. Exp. Med. *208*, 1367–1376.

34. Sutendra, G., Kinnaird, A., Dromparis, P., Paulin, R., Stenson, T.H., Haromy, A., Hashimoto, K., Zhang, N., Flaim, E., and Michelakis, E.D. (2014). A nuclear pyruvate dehydrogenase complex is important for the generation of acetyl-CoA and histone acetylation. Cell *158*, 84–97.

35. Paik, W.K., Pearson, D., Lee, H.W., and Kim, S. (1970). Nonenzymatic acetylation of histones with acetyl-CoA. Biochim. Biophys. Acta *213*, 513–522.

36. Nagampalli, R.S.K., Quesñay, J.E.N., Adamoski, D., Islam, Z., Birch, J., Sebinelli, H.G., Girard, R.M.B., Ascenção, C.F.R., Fala, A.M., Pauletti, B.A., et al. (2018). Human mitochondrial pyruvate carrier 2 as an autonomous membrane transporter. Sci. Rep. *8*, 3510.

37. Colca, J.R., McDonald, W.G., Cavey, G.S., Cole, S.L., Holewa, D.D., Brightwell-Conrad, A.S., Wolfe, C.L., Wheeler, J.S., Coulter, K.R., Kilkuskie, P.M., et al. (2013). Identification of a mitochondrial target of thiazolidinedione insulin sensitizers (mTOT)–relationship to newly identified mitochondrial pyruvate carrier proteins. PLoS One *8*, e61551.

38. Divakaruni, A.S., Wiley, S.E., Rogers, G.W., Andreyev, A.Y., Petrosyan, S., Loviscach, M., Wall, E.A., Yadava, N., Heuck, A.P., Ferrick, D.A., et al. (2013). Thiazolidinediones are acute, specific inhibitors of the mitochondrial pyruvate carrier. Proc. Natl. Acad. Sci. USA. *110*, 5422–5427.

39. Ramstead, A.G., Wallace, J.A., Lee, S.H., Bauer, K.M., Tang, W.W., Ekiz, H.A., Lane, T.E., Cluntun, A.A., Bettini, M.L., Round, J.L., et al. (2020). Mitochondrial pyruvate carrier 1 promotes peripheral T cell homeostasis through metabolic regulation of thymic development. Cell Rep. *30*, 2889–2899.e6.

40. Koishi, M., Yokota, S., Mae, T., Nishimura, Y., Kanamori, S., Horii, N., Shibuya, K., Sasai, K., and Hiraoka, M. (2001). The effects of KNK437, a novel inhibitor of heat shock protein synthesis, on the acquisition of thermotolerance in a murine transplantable tumor in vivo. Clin. Cancer Res. *7*, 215–219.

41. van Loosdregt, J., Fleskens, V., Fu, J., Brenkman, A.B., Bekker, C.P.J., Pals, C.E.G., Meerding, J., Berkers, C.R., Barbi, J., Gröne, A., et al. (2013). Stabilization of the transcription factor Foxp3 by the deubiquitinase USP7 increases Treg-cell-suppressive capacity. Immunity *39*, 259–271.

42. van Loosdregt, J., Fleskens, V., Tiemessen, M.M., Mokry, M., van Boxtel, R., Meerding, J., Pals, C.E.G., Kurek, D., Baert, M.R.M., Delemarre, E.M., et al. (2013). Canonical Wnt signaling negatively modulates regulatory T cell function. Immunity *39*, 298–310.

43. Fox, C.J., Hammerman, P.S., and Thompson, C.B. (2005). Fuel feeds function: energy metabolism and the T-cell response. Nat. Rev. Immunol. *5*, 844–852.

44. Gerriets, V.A., and Rathmell, J.C. (2012). Metabolic pathways in T cell fate and function. Trends Immunol. *33*, 168–173.

45. Jones, R.G., and Thompson, C.B. (2007). Revving the engine: signal transduction fuels T cell activation. Immunity *27*, 173–178.

46. Cham, C.M., and Gajewski, T.F. (2005). Glucose availability regulates IFN-gamma production and p70S6 kinase activation in CD8+ effector T cells. J. Immunol. *174*, 4670–4677.

47. Macintyre, A.N., Gerriets, V.A., Nichols, A.G., Michalek, R.D., Rudolph, M.C., Deoliveira, D., Anderson, S.M., Abel, E.D., Chen, B.J., Hale, L.P., and Rathmell, J.C. (2014). The glucose transporter Glut1 is selectively essential for CD4 T cell activation and effector function. Cell Metabol. *20*, 61–72.

48. Blagih, J., Coulombe, F., Vincent, E.E., Dupuy, F., Galicia-Vázquez, G., Yurchenko, E., Raissi, T.C., van der Windt, G.J.W., Viollet, B., Pearce, E.L., et al. (2015). The energy sensor AMPK regulates T cell metabolic adaptation and effector responses in vivo. Immunity *42*, 41–54.

49. Ho, P.C., Bihuniak, J.D., Macintyre, A.N., Staron, M., Liu, X., Amezquita, R., Tsui, Y.C., Cui, G., Micevic, G., Perales, J.C., et al. (2015). Phosphoenolpyruvate is a metabolic checkpoint of anti-tumor T cell responses. Cell *162*, 1217–1228.

50. Takahashi, H., McCaffery, J.M., Irizarry, R.A., and Boeke, J.D. (2006). Nucleocytosolic acetyl-coenzyme a synthetase is required for histone acetylation and global transcription. Mol. Cell *23*, 207–217.

51. Menk, A.V., Scharping, N.E., Moreci, R.S., Zeng, X., Guy, C., Salvatore, S., Bae, H., Xie, J., Young, H.A., Wendell, S.G., and Delgoffe, G.M. (2018). Early TCR signaling induces rapid aerobic glycolysis enabling distinct acute T cell effector functions. Cell Rep. *22*, 1509–1521.

52. Leticia Soriano-Baguet, M.G., Henry, K., Benzarti, M., Binsfeld, C., Ewen, A., Lynn, B., Guerra, L., Franchina, D.G., Kobayashi, T., Joseph, L., et al.

(2023). Pyruvate dehydrogenase fuels a critical citrate pool that is essential for Th17 cell effector functions. Cell Rep. *42*, 112153.

53. Schell, J.C., Wisidagama, D.R., Bensard, C., Zhao, H., Wei, P., Tanner, J., Flores, A., Mohlman, J., Sorensen, L.K., Earl, C.S., et al. (2017). Control of intestinal stem cell function and proliferation by mitochondrial pyruvate metabolism. Nat. Cell Biol. *19*, 1027–1036.

54. Li, H., and Durbin, R. (2009). Fast and accurate short read alignment with Burrows-Wheeler transform. Bioinformatics *25*, 1754–1760.

55. Tarasov, A., Vilella, A.J., Cuppen, E., Nijman, I.J., and Prins, P. (2015). Sambamba: fast processing of NGS alignment formats. Bioinformatics *31*, 2032–2034.

56. Zhang, Y., Liu, T., Meyer, C.A., Eeckhoute, J., Johnson, D.S., Bernstein, B.E., Nusbaum, C., Myers, R.M., Brown, M., Li, W., and Liu, X.S. (2008). Model-based analysis of ChIP-seq (MACS). Genome Biol. *9*, R137.

57. Ross-Innes, C.S., Stark, R., Teschendorff, A.E., Holmes, K.A., Ali, H.R., Dunning, M.J., Brown, G.D., Gojis, O., Ellis, I.O., Green, A.R., et al. (2012). Differential oestrogen receptor binding is associated with clinical outcome in breast cancer. Nature *481*, 389–393.

STAR★METHODS

KEY RESOURCES TABLE

REAGENT or RESOURCE	SOURCE	IDENTIFIER
Antibodies		
Anti-Human CD25-FITC Clone MEM-181	Immunotools	Cat# 21270253,
Anti-Human CD38- PerCP/Cyanine5.5	BioLegend	Cat# 303522; RRID: AB_893316
Anti-Human Semaphorin 7A-APC	Biotechne	Cat# FAB20681A
Anti-Human-CD3	eBioscience	Cat# 16-0037; RRID: AB_468854
Anti-human CD28	eBioscience	Cat# 16-0289-85; RRID: AB_468926
Anti-Mouse CD28 Functional	eBioscience	Cat# 16-0281-85; RRID: AB_468921
Anti-mouse CD3	eBioscience	Cat# 16-0031-85; RRID: AB_468847
Anti-mouse CD25 pacific blue	biolegend	Cat# 102022; RRID: AB_493643
Anti-mouse CD38-PE	biolegend	Cat# 102707; RRID: AB_312928
Anti-mouse CD69-APC	biolegend	Cat# 104513; RRID: AB_492844
FOXP3 Monoclonal Antibody (FJK-16s), FITC,	eBioscience, Invitrogen	Cat# 11577380
Anti-Mouse CD4-APC	Biolegend	Cat# 17-0041-81; RRID: AB_469320
Anti-mouse CD8- Brilliant Violet 570	biolegend	Cat# 100739; RRID: AB_10897645
Anti-mouse CD45-Pacific Blue	biolegend	Cat# 109820; RRID: AB_492872
Anti-mouse CD45RB-Pacific Blue	biolegend	Cat# 103315; RRID: AB_2174406
Anti-mouse CD138-APC	biolegend	Cat# 142505; RRID: AB_10962911
PE-Cy^{TM}7 Mouse Anti-Human IFN-γ	biolegend	Cat# 561036; RRID: AB_396894
PE/Cyanine7 anti-mouse IFN-γ Antibody	Biolegend	Cat# 505825; RRID: AB_2295770
goat anti- rabbit IgG alexa fluor 568	Molecular probes	Cat# A21069; RRID:AB_2535730
anti-mouse/human CD11b-PE	biolegend	Cat# 101207; RRID: AB_312790
Total Histone 3	cell signaling	Cat# 9715S
Anti-Histone H3-acetyl K27	Abcam	Cat# ab4729
Anti-trimethyl-Histone H3 K27	Millipore	Cat# 07-449
Histone H3K4me3 antibody	active motif	Cat# 39159; RRID: AB_2615077
Anti-Histone H3 (mono methyl K4)	Abcam	Cat# ab176877
Anti-Pyruvate Dehydrogenase E1-alpha subunit antibody	Abcam	Cat# ab110334
Anti-Actin	Santa Cruz	Cat# sc-1616
Anti-ACC2	Abcam	Cat# ab66038
Anti-Cox-2	Cayman	Cat#160112
PDHE1-Antibody	Proteintech	Cat# 18068-1-AP
ATP-Citrate lyase Ab	Cell Signaling	Cat# 4332
Chemicals, peptides, and recombinant proteins		
PBS (1X) without Ca++, Mg++, 500ml	Lonza	# BE17-516F
FBS	Biowest	Cat# S1810-500 Lot# S14068S1810
Penicillin-Streptomycin	Gibco	# 15-140-122
L-Glutamine	Lonza	# BE17-605E
2-Mercaptoethanol	Gibco	# 11508916
Methanol	Sigma-Aldrich	# 1060351000
RPMI + glutamax	Gibco	# 61870044
RPMI 1640 Medium, no glucose	Gibco	# 11879020
2-Deoxy-D-glucose	Sigma-Aldrich	# D8375-5G
oligomycin	Merck Millipore	# 495455
D-(+)-Galactose	Merck Millipore	# 48260

(*Continued on next page*)

Continued

REAGENT or RESOURCE	SOURCE	IDENTIFIER
FCCP, mitochondrial oxidative phosphorylation uncoupler	Abcam	# ab120081
Rotenone	Merck Millipore	# R8875
UK-5099 (Synonyms: PF-1005023)	Med Chem Express	# HY-15475
3PO ≥98% (HPLC)	Sigma-Aldrich	# SML1343
Sodium acetate	Sigma-Aldrich	# S1429
DCA	Tocris Bioscience	# 2755
Etomoxir sodium salt hydrate	Sigma-Aldrich	# E1905
ACSS2 inhibitor	Selleck	# S8588
6,8-Bis(benzylthio)-octanoic acid	Sigma-Aldrich	# SML0404
Sodium Pyruvate	Thermo Fisher	# 11360070
SB204990	Med Chem Express	# HY-16450
BMS303141	Sigma-Aldrich	# SML0784
HEPES	Sigma-Aldrich	#H4034-100G
EDTA	Sigma-Aldrich	#EDS-100G
DL-Dithiothreitol solution (DTT)	Sigma-Aldrich	#43816-10ML
Bovine serum albumin (BSA)	Sigma-Aldrich	#A9647-500G
D-(+)-Glucose solution	Sigma-Aldrich	#G8769-100ML
$^{13}C_6$-glucose	Cambridge Isotope Lab	#CLM-1396
DMSO	Sigma-Aldrich	# D2650
Ficoll® Paque Plus	Sigma-Aldrich	# GE17-1440-02
$^{13}C_6$-glucose	Cambridge Isotope Lab	#CLM-1396
Cell Trace Violet	Invitrogen	#C34557
Molecular Probes™ 2-NBDG	Invitrogen	#N13195
SYBR	Thermo fisher	#S33102
iScript cDNA kit	biorad	#170-8891
Formaldehyde	Sigma-Aldrich	#252549-1L
DAPI (1:2000)	Invitrogen	#D1306
Zombie NIR™ Fixable Viability Kit	Biolegend	#423106
Zombie Green™ Fixable Viability Kit	Biolegend	#423112
7-AAD	Invitrogen	#A1310
D-(+)-Glucose solution	Sigma-Aldrich	#G8769-100ML
GolgiPlug™ (Protein Transport Inhibitor)	BD Biosciences	#555029
Tween 20	Sigma-Aldrich	#P7949-500ML
HALT protease inhibitor	Thermo scientific	#78439
Powdered milk	Carl Roth	#T145.2
Pierce™ Protein A/G Magnetic Beads	thermo fisher	#88802
Proteinase K, recombinant, PCR Grade	Sigma	#3115828001
RNeasy Mini Kit	Qiagen	#74106
Seahorse XF DMEM medium	Agilent Technologies	#103575-100
Critical commercial assays		
MagniSortTM Human CD4+ T cell Enrichment Kit	eBioscience	#8804-6811-74
CD4 (L3T4) MicroBeads, mouse	Miltenyi	# 130-117-043
Duolink® In Situ Detection Reagents Red	Sigma	DUO92008
Duolink Green PLA	Sigma	# DUO92014
Foxp3/Transcription Factor Staining Buffer Set	eBioscience	#00-5523-00
BD Cytofix/Cytoperm Fixation/Permeabilization kit	BD Biosciences	#554714
seahorse XFe24 Flux Packs	Agilent	#1023-40-100
Acetyl-CoA Assay Kit	Biovision, Milpitas CA	#K317-100

(*Continued on next page*)

Continued		
REAGENT or RESOURCE	SOURCE	IDENTIFIER
nuclear extract kit	active motif	#40010
chip DNA clean & concentrator	zymo research	#D5205
IL2 elisa	Biolegend	#431804
EAE induction kit: MOG35-55/CFA Emulsion PTX	Hooke Laboratories, Inc	#EK-2110
Deposited data		
RNA-seq Pdha1 ko and Acly ko	This manuscript	GEO: GSE225875
RNA-seq and Chip seq human T cells	This manuscript	EGA: EGAS00001007115
Experimental models: Organisms/strains		
Mouse: B6(129X1)-Tg(Cd4-cre/ERT2)11Gnri/J	Jackson Laboratory	Jax: #022356
Mouse: Pdha1fl/fl	Jackson Laboratory	JAX: 017443, PMID: 29560354
Mouse: CD4-Cre Mpc1fl/fl	Ryan M. O'Connell Lab	N/A
Mouse: CD4-Cre ACLYfl/fl	Martin Vaeth Lab	N/A
Oligonucleotides		
See Table S1	Sigma	This Study

RESOURCE AVAILABILITY

Lead contact

Further information and requests for resources or reagents should be directed to and will be made available upon reasonable request by the Lead Contact: p.j.coffer@umcutrecht.nl

Materials availability

All unique/stable reagents generated in this study are available from the lead contact without restriction.

Data and code availability

- RNA-seq on the T cells isolated from Pdha1 ko and Acly ko mice have been deposited at GEO and are publicly available as of the date of publication. Accession number: GSE225875.
- The RNA-seq and Chip seq that were generated on this study with human T cells were deposit on EGA for the legal restriction of The Netherlands to share human DNA sequencing data. EGA study ID is : EGAS00001007115
- All other data reported in this paper will be shared by the lead contact upon request.
- This paper does not report original code.
- Any additional information required to reanalyze the data reported in this paper is available from the lead contact upon request.

EXPERIMENTAL MODEL AND STUDY PARTICIPANT DETAILS

Pdha1 T cell-specific KO mice

Mice described in these studies received care at the University of Alberta according to the Canadian Council on Animal Care and all procedures were approved by the University of Alberta Health Sciences Animal Welfare Committee. To generate *Pdha1*$^{CD4+KO}$ mice, transgenic mice expressing tamoxifen-inducible Cre in CD4 T cell (CD4^{CreERT2}) were crossed with *Pdha1*$^{fl/fl}$ mice (PMID: 29560354) (stock no. 017443; The Jackson Laboratories). Cre-induced activation of the knockout was carried out through 5 consecutive intraperitoneal (i.p.) injections of tamoxifen (100 mg/kg/day) in male mice starting at 6 weeks of age. All mice were allowed 3 weeks washout post-tamoxifen administration prior to experimentation.

MPC1 T cell-specific KO mice

Mice described in these studies are on the C57BL/6 genetic background and were housed in the animal facility at the University of Utah. Mpc1 floxed mice were described previously[39,53] and crossed to CD4-Cre mouse strains obtained from Jackson laboratories. Mice were age and sex-matched male for all experiments with an age range of 6-12 weeks old. All experiments were approved by the Institutional Animal Care and Use Committee at the University of Utah.

ACLY T cell-specific KO mice

All mice were bred and maintained under specific pathogen-free conditions at the Center for Experimental Medicine (ZEMM) or the Institute for Systems Immunology at the Julius-Maximilians University of Würzburg. ACLY Cd4Cre mice were described previously[21]. Mice males were used for all experiments with an age range of 6-12 weeks old. All animal protocols were approved by government of Lower Franconia, Germany.

Collection of PB samples

Peripheral blood (PB) was collected from anonymous healthy donors (Hc) enrolled in the Minidonor Dienst Program at the UMC Utrecht after prior informed consent from each donor. The age range of the donors is unknown, but it is estimated to be between 25 and 60 years old. Additionally, as gender is not disclosed, it is unclear whether the samples were obtained from male or female individuals. PB was drawn at the same moment via vein puncture or intravenous drip. The study procedures were approved by the Institutional Review Board of the University Medical Center Utrecht (UMCU; METC nr: 11-499c) and performed according to the principles expressed in the Helsinki Declaration. Peripheral blood mononuclear cells (PBMCs) were isolated using Ficoll Isopaque density gradient centrifugation (GE Healthcare Bio-Sciences AB) and were used fresh or after freezing in FCS (Invitrogen) containing 10% DMSO (Sigma-Aldrich).

METHOD DETAILS

Human T cell isolation and culture

$CD4^+$ T cells were isolated from PBMCs using MagniSortTM Human $CD4^+$ T cell Enrichment Kit (eBioscience 8804-6811-74). The $CD4^+$ T cells were cultured always in RPMI Medium 1640 + GlutaMAX supplemented with 100 U/ml penicillin, 100 mg/ml streptomycin (all obtained from Life Technologies), and 10% heat-inactivated human AB-positive serum (Invitrogen) at 37°C in 5% CO2. Where indicated, $CD4^+$ T cells were activated with 1 μg/ml plate-bound anti-CD3 (eBioscience; 16-0037) and 1 μg/ml anti-CD28 (eBioscience; 16-0289-85) during 12, 24 or 48 hours. Where indicated cells were treated with Oligomycin (1μM Sigma Aldrich), 2DG (50mM Sigma Aldrich), Galactose (10mM Sigma Aldrich), 3PO (50μM Sigma Aldrich), UK-5099 (5uM Sigma Aldrich), DCA (5mM Tocris Bioscience), Etomoxir (3uM, 5uM, and 10uM Sigma Aldrich), SB204990 (Med Chem Express), BMS303141 (Sigma Aldrich), ACSS2-Inhibitor (15uM Selleck) 6,8-Bis(benzylthio) octanoic acid (Sigma Aldrich), Na-pyruvate 2mM or Acetate (20mM).

Chromatin-immunoprecipitation

For each sample, cells were crosslinked with 2% formaldehyde and crosslinking was stopped by adding 0.2 M glycine. Nuclei were isolated in 50 mM Tris (pH 7.5), 150 mM NaCl, 5 mM EDTA, 0.5% NP-40, and 1% Triton X-100 and lysed in 20 mM Tris (pH 7.5), 150 mM NaCl, 2 mM EDTA, 1% NP-40, 0.3% SDS. Lysates were sheared using Covaris microTUBE (duty cycle 20%, intensity 3, 200 cycles per burst, 60-s cycle time, eight cycles) and diluted in 20 mM Tris (pH 8.0), 150 mM NaCl, 2 mM EDTA, 1% X-100. Sheared DNA was incubated overnight with anti-histone H3 acetyl K27 antibody (ab4729; Abcam) pre-coupled to protein A/G magnetic beads. Beads were washed and crosslinking was reversed by adding 1% SDS, 100 mM NaHCO3, 200 mM NaCl, and 300 mg/ml proteinase K. DNA was purified using ChIP DNA Clean & Concentrator kit (Zymo Research). The Chip DNA was used for sequencing or qPCR

DNA/RNA-sequencing

End repair, a-tailing, and ligation of sequence adaptors were done using Truseq nano DNA sample preparation kit (Illumina). Samples were PCR amplified, checked for the proper size range, and for the absence of adaptor dimers on a 2% agarose gel, and barcoded libraries were sequenced 75 bp single-end on Illumina NextSeq500 sequencer (Utrecht DNA sequencing facility). Total cellular RNA was extracted using the RNAeasy kit (QIAGEN). Sample preparation was performed using TruSeq stranded total RNA with ribo-zero globin sample preparation kit (Illumina), and samples were sequenced 75 bp single-end on Illumina NextSeq500 (Utrecht DNA sequencing facility).

ChIP-qPCR

Real-time PCR was performed with PowerSYBR (Applied Biosystems) using a StepOnePlus Real-Time-PCR system (Applied Biosystems). The expression of each gene was normalized to a negative region. All the primers for the Chip-qPCR they were designed based on or Chip-seq. All primers utilized in this paper are specified in the supplemental Excel file Table S1.

Detection of apoptosis

Apoptosis was determined with Annexin V-PE apoptosis detection kit (BD Biosciences). Stained cells were acquired by FACS using an LSRII (Becton Dickinson) and data were analyzed with FlowJo software (Tree Star, Inc). Or counting the cells with Bio-Rad® TC20 Automated cell counter in presence of Trypan blue.

Immunoblotting

Total cellular lysates were prepared using RIPA buffer (1% Triton-X 100, 1% sodium deoxycholate, 0.1%SDS, 0.15 M NaCl, 0.01 M sodium phosphate, pH 7.2). Membranes were incubated with the following primary antibodies: Total Histone 3 (H3, cell signaling; 9715S), Anti-Histone H3-acetyl K27 (H3AcK27, Abcam; ab4729), Anti-trimethyl-Histone H3 K27 (H3K27met^{3}, Millipore; 07-449), Histone H3K4me3 antibody (H3K4met^{3}, active motif 39159), Anti-Histone H3 (mono methyl K4) antibody (H3K4met^{1} , Abcam; ab176877), Anti-Pyruvate Dehydrogenase E1-alpha subunit antibody (PDH1, Abcam; ab110334), Anti-Actin (Santa Cruz; sc-1616). Anti-ACC2 (ACC2, Abcam; ab66038), ATP-Citrate lyase Ab (ACLY, Cell Signaling;4332), and Anti-Cox-2 (Cayman; 160112).

Real-time PCR

RNA was isolated from cells using RNeasy Mini Kit (Qiagen) and cDNA was synthesized using Superscript-III First-Strand Synthesis System (Life Technologies). Real-time PCR was performed with PowerSYBR (Applied Biosystems) using a StepOnePlus Real-Time-PCR system (Applied Biosystems). Expression of each gene was normalized to β2M. All primers utilized in this paper are specified in the supplemental Excel file Table S1.

Seahorse assay

T cells were stimulated with anti-CD3 and anti-CD28 for 12, 24, and 48 hours. Oxygen consumption rates (OCR) and extracellular acidification rates (ECAR) were measured in XF media (non-buffered RPMI 1640 containing 10 mM glucose, 2 mM L-glutamine, and 1 mM sodium pyruvate) under basal conditions and in response to glucose 30mM, 1uM oligomycin, and 50mM of 2DG, on an XF-24 Extracellular Flux Analyzers (Seahorse Bioscience).

Measurements of acetyl-coA levels

The intracellular levels of acetyl-CoA were detected by using an Acetyl-CoA Assay Kit (Biovision, Milpitas CA), following the manufacturer's instructions.

Measurement of pyruvate levels using liquid chromatography-mass spectrometry (LC-MS) based metabolomics

T cells were seeded at a density of 1*10^{6} cells/ml in RPMI (10% FBS) by supplemented with 11 mM [U-^{13}C]D-Glucose (Cambridge Isotopes). T cells were stimulated in the presence or absence of 2-DG. After 3, 6, 16, 24 hours, 5*10^{5} cells were harvested, centrifuged for 5 min 1000xG, and the cell pellet was washed with ice-cold PBS. Metabolites were extracted by adding 50 μl ice-cold MS lysis buffer (methanol/acetonitrile/ULC/MS grade water (2:2:1)) to the cell pellet. Samples were shaken for 10 minutes at 4°C, centrifuged at 14.000g for 15 min at 4°C, and supernatants were collected for LC-MS analysis. LC-MS analysis was performed on an Exactive mass spectrometer (Thermo Scientific) coupled to a Dionex Ultimate 3000 autosampler and pump (Thermo Scientific). The MS operated in polarity-switching mode with spray voltages of 4.5 kV and -3.5 kV. Metabolites were separated using a Sequant ZIC-pHILIC column (2.1 x 150 mm, 5 μm, guard column 2.1 x 20 mm, 5 μm; Merck) using a linear gradient of acetonitrile and eluent A (20 mM (NH4)2CO3, 0.1% NH4OH in ULC/MS grade water (Biosolve)). The flow rate was set at 150 μl/min. Metabolites were identified and quantified using LCquan software (Thermo Scientific) based on exact mass within 5 ppm and further validated by concordance with retention times of standards.

Incorporation of glucose-derived carbons in histones measured by liquid chromatography-mass spectrometry (LC-MS) based proteomics

Bands corresponding to the MW of histones were excised from the polyacrylamide gel, after which they were destained with 50% Acetonitrile (ACN). After reduction with 10 mM Tris (2-carboxyethyl) phosphine hydrochloride (TCEP) in 50mM Ammonium Bicarbonate (ABC), proteins were alkylated in the dark with 40mM Chloro-Acetamide. After digestion with 200 ng Tryp/LysC protease mix (Promega) in 50mM ABC, peptides were desalted on homemade C18 stage tips (3M, St Paul, MN). After elution from the stage tips, acetonitrile was removed using a SpeedVac and the remaining peptide solution was diluted with buffer A (0.1% FA) before loading. Peptides were separated on a 30 cm pico-tip column (75μm ID, New Objective) in-house packed with 1.9 μm aqua pure gold C-18 material (dr. Maisch) using 240 gradients (7% to 80% ACN 0.1% FA), delivered by an easy-nLC 1000 (Thermo), and electro-sprayed directly into an Orbitrap Fusion Tribrid Mass Spectrometer (Thermo Scientific). The latter was set in data-dependent Top speed mode with a cycle time of 1 second, in which the full scan over the 400-1500 mass range was performed at a resolution of 240000. Most intense ions (intensity threshold of 5000 ions) were isolated by the quadrupole and fragmented with an HCD collision energy of 30%. The maximum injection time of the ion trap was set to 50 milliseconds with injection of ions for all available parallelizable time. Raw files were analyzed with the Maxquant software version 1.6.10.43 (Cox and Mann, 2008) with acetylation of lysines as well as oxidation of methionine set as variable modifications, and carbamidomethylation of cysteine set as fixed modification. A protein database containing Histone H3 was searched with both the peptide as well as the protein false discovery rate set to 1%. Extracted chromatograms of the isotope cluster of the acetylated peptide of H3K27 were made using the software package Skyline (MacLean et al. 2010) (PMC2844992)The mass spectrometry proteomics data have been deposited to the ProteomeXchange Consortium via the PRIDE partner repository (http://www.ebi.ac.uk/pride) with the dataset identifiers (PXD018132).

Proximity ligation assay (PLA)

Cells were washed 3 times in PB and incubated in mouse PLUS and rabbit MINUS probes (Sigma Aldrich) according to the manufacturer's protocol. Cells were washed in PB before detection using the *in situ* PLA detection kit (Sigma-Aldrich) as previously described.[37] Samples were analyzed with a 63x objective on a Leica SP8X.

Isolation and culture of mouse naïve CD4$^+$ T cells

Spleens were removed from mice, homogenized, and filtered through a 40 μM filter. Red blood cells were then lysed with RBC lysis buffer (Biolegend). Splenocytes were stained with fluorescent antibodies and naïve CD4$^+$ T cells (CD3$^+$ CD4$^+$ CD44$^-$) were purified from splenocytes using FACS sorting. Purified naïve CD4$^+$ T cells were then resuspended in RPMI media containing 10% FBS, L-glutamine, Pen/Strep antibiotics, HEPES, Sodium Pyruvate, and Non-essential amino acids. To activate CD4$^+$ T cells, a 96 well plate was coated with 200 μl/well of 5 μg/ml LEAF αCD3 (Biolegend) in PBS for at least 4 hours at 37°C. 1X10^5 splenic naïve CD4$^+$ T cells were cultured in the presence of coated αCD3 and 2 μg/ml of soluble LEAF αCD28 (Biolegend) for 24 hours. CD69 and CD25 expression were measured by flow cytometry. To measure gene expression of Mpc1, Sema7a, and Il2ra, cells were stored in Qiazol lysis reagent (Qiagen) and total RNA was isolated using the miRNeasy kit (Qiagen). Then, cDNA was made using the qScriptTM kit (QuantaBio) and qPCR was performed on an Applied Biosystems QuantStudio 6 Flex using PowerUp (Applied Biosystems) SYBR Green Master mix. Primers for mouse *Sema7a* and mouse CD25 (*Il2ra*) were acquired from the University of Utah DNA synthesis core and primers for mouse *Mpc1* were acquired from IDT. All primers utilized in this paper are specified in the supplemental Excel file 'Oligonucleotides Mocholi et al.

ChIP-seq analysis

Reads from all different ChIP-Seq libraries where aligned to the reference genome (GRCm38/mm10) with bwa[54] with the following settings : bwa mem -M -c 100. Duplicate marking was done using sambamba markdup[55]. Regions significantly enriched for H3K27ac compared with corresponding input control samples (both IP/treatment and control in triplo) were identified using the MACS2 peak caller[56] and the following parameters : -f BAMPE -g mm –nomodel –extsize 215 –bdg. Analysis of differential ChIP enrichment was done by analysing the MACS2 BED files with H3K27ac peak regions using the R/Bioconductor diffBind package[57]. Reads in peak regions were counted with the dba.counts method and subsequently normalized with the dba.normalize method using the "DBA_NORM_TMM" parameter. Contrasts for comparisons between WT and KO mice (both PDH and ACLY) were defined with dba.contrast and analysis and reporting were performed using the dba.analyze and dba.report methods.

QUANTIFICATION AND STATISTICAL ANALYSIS

For ChIP-seq and RNA-seq analysis, p values were adjusted with the Benjamini-Hochberg procedure. For ChIP-seq regions with a significantly different H3K27ac signal were defined using a false discovery rate (FDR) <0.05.

Data are presented as the mean±SEM with a minimum n=3 per group (for more information, please refer to the Figure Legends). P values were calculated using the unpaired Student's t test, or one or two-way ANOVA using Tukey test correction for multiple comparisons, and Prism 9.3.1 (GraphPad). Statistical significance was set at $p \leq 0.05$, with levels indicated by asterisks as follows: * $p \leq 0.05$; ** $p \leq 0.01$; *** $p \leq 0.001$; **** $p \leq 0.0001$; ns, not significant.